J. Fluid Mech. (1991), *vol.* 223, *pp.* 411–456
Printed in Great Britain

Nonlinear dynamics of viscoelastic flow in axisymmetric abrupt contractions

By GARETH H. McKINLEY, WILLIAM P. RAIFORD, ROBERT A. BROWN AND ROBERT C. ARMSTRONG

Department of Chemical Engineering, Massachusetts Institute of Technology, Cambridge, MA 02139, USA

(Received 6 February 1990)

The steady-state and time-dependent flow transitions observed in a well-characterized viscoelastic fluid flowing through an abrupt axisymmetric contraction are characterized in terms of the Deborah number and contraction ratio by laser-Doppler velocimetry and flow visualization measurements. A sequence of flow transitions are identified that lead to time-periodic, quasi-periodic and aperiodic dynamics near the lip of the contraction and to the formation of an elastic vortex at the lip entrance. This lip vortex increases in intensity and expands outwards into the upstream tube as the Deborah number is increased, until a further flow instability leads to unsteady oscillations of the large elastic vortex. The values of the critical Deborah number for the onset of each of these transitions depends on the contraction ratio β, defined as the ratio of the radii of the large and small tubes. Time-dependent, three-dimensional flow near the contraction lip is observed only for contraction ratios $2 \leqslant \beta \leqslant 5$, and the flow remains steady for higher contraction ratios. Rounding the corner of the 4:1 abrupt contraction leads to increased values of Deborah number for the onset of these flow transitions, but does not change the general structure of the transitions.

1. Introduction

Viscoelastic fluid flows in many complex geometries are observed to develop instabilities at low flow rates which are absent in the flow of purely Newtonian liquids. These instabilities develop at very low Reynolds numbers and depend solely on the elastic nature of the fluid. Elastic instabilities have been observed in many flows including Taylor–Couette flow (Giesekus 1972; Larson, Shaqfeh & Muller 1990), flow around a sphere (Bisgaard 1983), flow in a cone-and-plate rheometer (Magda & Larson 1988) and motion in a variety of entry flows (Boger 1982, 1987). The great variety of nonlinear transitions that have been observed qualitatively and the importance of many of these complex flows in industrial processing of polymers, coatings, and colloidal systems has been a large part of the motivation for the intense interest in numerical simulation of viscoelastic flows using a variety of constitutive equations.

Although very motivating, few of these experiments have been quantitative enough to provide benchmarks for comparison with theory and computations. Such comparisons are an important next step in the development of the fluid mechanics of viscoelastic liquids. To meet this objective, the experiments must be carried out with a rheologically well-characterized fluid and must be accurate enough to describe

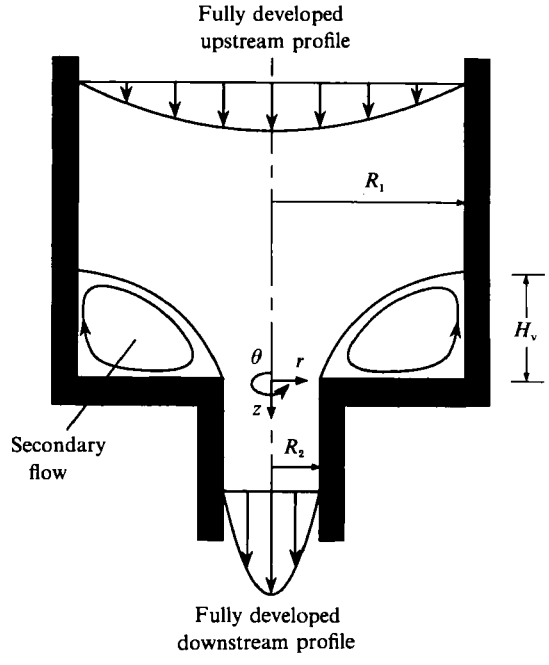

FIGURE 1. Schematic diagram of the axisymmetric contraction geometry. The contraction ratio is defined as $\beta = R_1/R_2$ and the dimensionless vortex reattachment length is $\chi \equiv H_v/2R_1$.

sufficiently both the spatial and temporal symmetries of the flow and provide quantitative measurements that can be directly compared with calculations. The highly accurate technique of laser-Doppler velocimetry (LDV) has been used with great success in earlier investigations of inertial instabilities in Newtonian flows. The wide dynamic range and non-invasive features of laser-Doppler velocimetry have permitted accurate documentation of the complex sequence of hydrodynamic transitions leading to time-dependent flow regimes in Taylor–Couette flow and Rayleigh–Bénard convection (Fenstermacher, Swinney & Gollub 1979; Gollub & Benson 1980). In this paper we use the LDV technique coupled with conventional flow visualization methods to document the sequence of nonlinear transitions observed in the creeping flow of a highly elastic, non-Newtonian fluid through an abrupt axisymmetric contraction.

The basic geometry for an abrupt axisymmetric contraction flow is shown in figure 1 and consists of a large upstream tube of radius R_1 which contracts suddenly to a smaller tube with radius R_2. The fluid accelerates from a fully developed upstream profile to another fully developed profile at some distance downstream of the contraction plane. A recirculating secondary flow may also be present in the corners of the large tube immediately upstream of the contraction plane, depending on the flow rate and rheology of the viscoelastic fluid. Such entry flows contain significant shearing and extensional components and are encountered commonly in many commercially important polymer processing applications, such as extrusion and fibre spinning. In each case processing limits are encountered at low Deborah numbers owing to the onset of unstable flow regimes; see Petrie & Denn (1976) for a review of flow instabilities in polymer processing.

The fluid mechanics of contraction flows is one of the most thoroughly studied

experimental systems for complex viscoelastic motion and has been reviewed in detail by Boger (1982, 1987) and by White, Gotsis & Baird (1987). A myriad of interesting flow phenomena have been observed with increasing Deborah numbers. As the flow rate through the contraction is increased a viscoelastic fluid undergoes transitions from the low-flow-rate, Newtonian-like behaviour to regimes which may exhibit greatly enhanced vortex size or streamlines that diverge away from the centreline at some distance above the contraction plane. At high flow rates the large vortex observed in many viscoelastic entry flows ultimately becomes unstable, resulting in large fluctuations in the flow field and gross distortion of the viscoelastic material downstream of the contraction. It has also been observed by several authors (Lawler *et al.* 1986; Boger, Hur & Binnington 1986; Evans & Walters 1986, 1989; Raiford *et al.* 1989) that these transitions may proceed via the formation of an independent elastic lip vortex at the re-entrant corner where the upstream tube joins the downstream tube.

These previous investigations have yielded the first glimpses of the rich nonlinear structure of contraction flows and have demonstrated the sensitive dependence of the observed flow transitions on the following parameters: the contraction ratio, the viscoelastic fluid rheology for both polymer melts and solutions, the details of the flow geometry including whether it is planar or axisymmetric, and the precise shape of the contraction lip, i.e. whether it is sharp or rounded. The comprehensive reviews by Boger (1987) and White *et al.* (1987) describe these effects in greater detail.

The formation of the secondary flows is so pronounced that the flow through an axisymmetric contraction has been made a benchmark problem for numerical simulations of viscoelastic flows (Hassager 1988). Unfortunately the violent effects on the velocity and stress fields caused by rapid acceleration of the fluid through the contraction, especially near the re-entrant corner, make this problem extremely difficult, and reliable numerical results at moderate Deborah numbers are only just beginning to appear (Marchal & Crochet 1987; Coates, Armstrong & Brown 1991).

The importance of fluid elasticity in these flow transitions has been characterized by the Deborah number defined as

$$De = \frac{\lambda}{\mathscr{T}}, \tag{1}$$

where λ is a characteristic relaxation time for the viscoelastic fluid and $\mathscr{T}$ is the characteristic residence time for the flow geometry. The viscoelastic flow transitions described here develop at very low Reynolds numbers and at values of the Deborah number between 1 and 10.

In the past, most experimental investigations of these transitions have either involved qualitative techniques such as flow visualization or have attempted to correlate macroscopically observable quantities, e.g. excess pressure drop or vortex size, with flow parameters such as the Reynolds number and Deborah number to measure the relative importance of inertia and elasticity in the flow. Cable & Boger (1978*a*, *b*, 1979) investigated in great detail the flow of shear-thinning polymer solutions through axisymmetric contractions. They documented three distinct stable flow regimes as the flow rate was increased: a *Newtonian-like* creeping flow at very low flow rates, a *vortex growth* regime with a large steady recirculating vortex in the large upstream tube at moderate flow rates, and a *diverging flow* regime at higher flow rates with the streamlines diverging away from the centreline. At a particular Deborah number the upstream flow became unstable and the large vortex was observed either to pulse symmetrically or develop an asymmetry and spiral around

the upstream tube depending on the flow conditions. By varying the rheological properties of the test fluids and the experimental conditions the competing effects of elastic, viscous, and inertial forces were demonstrated. Fluid inertia was found to be stabilizing, requiring higher values of the Deborah number for the onset of flow instabilities.

Subsequent experiments by Nguyên & Boger (1979) used highly viscous, elastic fluids with viscosities that remain nearly constant over many decades of shear rate. These semi-dilute polymer solutions are known as *Boger* fluids (Boger 1977/78; Boger & Nguyên 1978) and consist of a small amount of high-molecular-weight polymer dissolved in a very viscous solvent. Rheological data presented for a number of different Boger fluid formulations (Prilutski *et al.* 1983; Jackson, Walters & Williams 1984; Binnington & Boger 1985) suggested that at low shear rates the viscometric properties could be modelled by the simple quasi-linear Oldroyd-B constitutive equation (Oldroyd 1950) which has subsequently been used extensively in numerical simulations. More recent experiments in transient shear flows (Mackay & Boger 1987; Quinzani *et al.* 1990) have shown that a spectrum of relaxation times is needed to model the rheological behaviour of Boger fluids over a wide range of shear rates.

The flow transitions observed in visualization experiments with Boger fluids by Nguyên & Boger agreed qualitatively with the observations for shear-thinning viscoelastic fluids. These results are described in some detail because of their relevance to the experiments presented here. At low flow rates ($De \ll 1$) the motion was essentially Newtonian, with a steady axisymmetric flow that converged radially into the small tube and a small corner vortex upstream of the contraction plane in the outer corner of the large tube. This corner vortex is strictly a result of the Newtonian stresses caused by the kinematical constraints of the corner and its presence is predicted by applying the similarity solution of Moffatt (1964) to analysis of the local flow in this region. The size of this vortex, as measured by the distance it extends up the wall of the large tube, agrees very well with the size determined from calculations for a Newtonian fluid (Kim-E, Brown & Armstrong 1983). Increasing the flow rate, and thereby raising the Deborah number, once again gave rise to a sequence of flow transitions which ultimately led to instabilities in the flow field. At moderate Deborah numbers ($De \sim 1$–3) the corner vortex increased greatly in size and expanded upstream. This large vortex then became asymmetric ($De \sim 5$) and at higher Deborah numbers ($De \sim 10$) began to spiral around the upstream tube, resulting in large fluctuations of the vortex height. Finally at $De \sim 15$ these oscillations became aperiodic.

The first quantitative measurements of the spatial and temporal structure in the nonlinear flow transitions which occur in a viscoelastic entry flow were presented by Muller (Muller 1986; Lawler *et al.* 1986). An automated two-colour laser-Doppler velocimetry system was used to study the flow of a highly elastic Boger fluid through a 4:1 abrupt axisymmetric contraction. The fluid was a solution of 0.17 wt% polyisobutylene (PIB) in polybutene (PB) with a zero-shear-rate relaxation time of 0.047 s. The most important result of this work was to show that at a relatively low critical Deborah number, $De^{(osc)} \approx 0.80$, the flow near the contraction lip became three-dimensional and all three velocity components exhibited time-dependent oscillations. The oscillation frequency was determined from the Fourier spectrum to be approximately 0.2 Hz and was found to increase with Deborah number. Hysteresis in the oscillation frequency was observed with a transition between the original time-periodic state and one with approximately twice the period. This behaviour may be indicative of a subcritical, period-doubling bifurcation. These oscillations were

confined to a small region near the contraction lip and were a precursor to the formation of a steady, two-dimensional, elastic vortex near the lip at a second critical Deborah number, $De^{(lip)} \approx 1.2$. Subsequent growth of this vortex could not be observed because of constraints to the maximum attainable Deborah number that were imposed by the fluid rheology and construction of the experimental system.

Visualization experiments reported by Boger *et al.* (1986) for 0.10 wt % PIB/PB solutions also showed the formation of an elastic vortex near the contraction lip that seemed to be time-dependent. More importantly these authors document that this elastic lip vortex grows with increasing *De* and develops into a large elastic vortex that expands into the large upstream tube at high Deborah numbers. The dynamics of this vortex are similar to that observed in the earlier experiments of Nguyên & Boger.

Studies by Boger and coworkers (Boger *et al.* 1986; Boger 1987) for different fluids and various contraction ratios have shown the sensitivity of the formation of the elastic lip vortex to these parameters. For example, for a particular PIB/PB Boger fluid the distinct lip vortex was seen only for contraction ratios less than 8:1. In higher contraction ratios the corner vortex expanded inwards towards the lip until it covered the contraction plane and subsequently grew upstream. However, for polyacrylamide (PAC)/cornsyrup (CS) Boger fluids a lip vortex is observed only in a 2:1 contraction. The large vortices observed in higher contraction ratios resulted from growth of the corner eddy, not from the formation of an independent lip vortex. The role of time-dependent dynamics near the contraction lip on the formation and growth of this elastic vortex is not known.

The differences in behaviour of the PIB/PB and PAC/CS Boger fluids in axisymmetric contractions has not been resolved, but may be caused by large differences in the extensional rheology of the two solutions. Experiments with polymer melts have shown conclusively that vortex growth occurs when the fluid exhibits a large increase in the uniaxial extensional viscosity with increased extension rate (White & Kondo 1977/78; White & Baird 1986). Reliable experimental data on the extensional rheology of Boger solutions is scarce; however, it appears that both PAC/CS and PIB/PB fluids do exhibit extremely high elongational viscosities (Jackson *et al.* 1984; Jones, Walters & Williams 1987; Walters 1989). Hence vortex growth is to be expected for both solutions, as is observed experimentally. The experimental results described below suggest that the differences between the behaviour of the PAC/CS and PIB/PB solutions for each contraction ratio may result solely from changes in the sequence of nonlinear transitions for the flow caused by differences in fluid rheology.

Here we report detailed laser-Doppler velocimetry measurements and flow visualization studies for the flow of a rheologically well-characterized Boger fluid through axisymmetric contractions with a wide range of contraction ratios ($2 \leqslant \beta \leqslant 8$). The Boger fluid is a semi-dilute solution of PIB in PB and is more elastic than the one used in the earlier experiments of Muller (Lawler *et al.* 1986). Higher values of Deborah number are attained, allowing measurements of the evolution of the elastic lip vortex into the large vortex described by Boger *et al.* (1986). The results show that the formation of the elastic lip vortex and its subsequent growth with increasing *De* may be accompanied by the onset of three-dimensional, time-dependent behaviour in the flow adjacent to the contraction lip. These temporal instabilities are highly localized and thus not readily observable by using other simple flow visualization procedures. Experiments with different contraction ratios demonstrate that the structure of the dynamic behaviour near the lip is not solely a

function of the local kinematics but also depends on the flow conditions in the large upstream tube. By systematically varying the contraction ratio in these experiments we show the competing effects of total extensional strain and shear rate in the upstream tube on the flow transitions near the lip. The importance of the severe flow conditions near the re-entrant corner and the effect of the corner on the dynamic structure of the flow has also been investigated by substituting a smooth radius of curvature for the sharp corner at the entrance to the small downstream tube.

2. Experimental

2.1. *Laser-Doppler velocimetry*

Laser-Doppler velocimetry (LDV) is a non-invasive technique for accurate measurement of point velocity components throughout a flow domain. In these experiments, a two-colour LDV system (TSI, Model 9100-12) is used to measure the axial, radial and tangential velocity components in an axisymmetric contraction. The system is fully automated and has been described in detail by Raiford (1989). In the current configuration velocities in the range 0.01–40 cm/s can be measured. The beams from a 4 W Argon-ion laser (Lexel, Model 95-4) are focused to form a measuring volume of dimensions $50 \times 50 \times 250$ μm and the entire optic train is mounted on a three-dimensional translating table (TSI, Model 9500) enabling accurate movement of the measuring volume throughout the flow geometry. It was found that the highly viscous polybutene solvent used in these experiments already contained a sufficient density of scattering sites and no additional seeding particles were required in the test fluid. Steady-state velocity data are analysed using a dual-channel Spectrum Analyzer (Nicolet, Model 660B) to determine the Doppler frequency of the light scattered by particles flowing through the measuring volume. The LDV system is also used to measure transient or time-dependent velocity fields by employing frequency trackers (DISA, Model 55N20/21) to follow the Doppler frequency of the scattered light. The analogue output signals from the trackers are then passed to the Spectrum Analyzer and a fast-Fourier transform (FFT) is calculated in real time to yield the frequency spectrum of any fluctuations in the velocity components. In all time series data presented here, the total observation time T is 400 s, and the spectral resolution of the FFT is thus $1/T \equiv 0.0025$ Hz.

The LDV technique has been used by several researchers (Yoganathan & Yarlagadda 1984; Lawler *et al.* 1986; Wunderlich, Brunn & Durst 1988 and Raiford *et al.* 1989) to evaluate quantitatively the steady-state kinematics of viscoelastic flow in planar and axisymmetric contractions. Lawler *et al.* demonstrated the accuracy of the experimentally measured velocity profiles by comparing their LDV results for a Newtonian fluid with the numerical finite-element simulations of Kim-E *et al.* (1983). Time-dependent velocity measurements in viscoelastic fluids have also been performed by Bisgaard (1983), Lawler *et al.* (1986) and Burdette (1989).

2.2. *Flow visualization*

The global flow dynamics were recorded on videotape by using a high-resolution video camera (Panasonic, Model D5000) with a macro lens (Minolta MD Macro 50 mm, f/3.5). The flow field was illuminated by passing a single blue beam from the Ar-ion laser through a cylindrical lens to form an expanded plane of laser light. This sheet of light is positioned perpendicularly to the camera to illuminate a longitudinal section of the contraction geometry. Long time exposure or 'streak' photographs were made to record the streamlines in the flow field. Streak photography has been

used extensively in previous experimental investigations to provide a qualitative representation of the streamlines in viscoelastic fluid flow through a number of complex geometries; see for example Walters & Webster (1982) and Binding *et al.* (1987).

2.3. *Flow circulation system and flow geometry*

The basic design for the fluids handling system has been described by Raiford (1989). The test fluid is circulated by a positive displacement pump (Moyno, Model no. 2L8) connected to a pressurized holding tank. From the tank the fluid passes through the test geometry and a valve network before emptying into an open collection tank. To eliminate the possibility of induced fluctuations in the flow, the recirculation pump is only used to recharge the 40-gallon holding tank and is not operated continuously. The fluid is forced through the test section solely by the static pressure driving force and the flow rate is controlled by adjustments to the valve system. In this mode of operation, experiments may be conducted continuously for approximately 1–2 h, depending on the flow rate.

The axisymmetric contraction test geometry is shown schematically in figure 1. The contraction ratio is defined as $\beta \equiv R_1/R_2$. In these experiments the downstream, small tube radius is maintained at $R_2 = 0.318$ cm ($\frac{1}{8}$ in.), and the contraction ratio is adjusted by inserting annular sheaths of varying internal radius (R_1) into the upstream tube. Contraction ratios of $\beta = 2$, 3, 4, 5, 6 and 8 have been studied. A cylindrical polar coordinate system (r, θ, z) with its origin located at the intersection of the symmetry axis and the contraction plane is used to specify position in the flow field. Positions upstream of the contraction plane correspond to $z < 0$. Dimensionless coordinates $\xi = r/R_2$ and $\zeta = z/R_2$ are used to compare results from different contraction ratios.

2.4. *Fluid rheology*

Highly elastic, constant-viscosity liquids such as the fluid described here were first formulated by Boger (1977/78) and have since been used extensively in experimental investigations of viscoelastic fluid flow. The high viscosities of these so-called Boger fluids minimize inertial effects whereas the long relaxation times, comparable to those measured in polymer melts, lead to high Deborah numbers in the flow experiments.

The viscoelastic test fluid used in these experiments is a Boger fluid consisting of a high-molecular-weight polyisobutylene (PIB) (Exxon Vistanex L-120, $M_w \approx 1.2 \times 10^6$ g/mol) which is dissolved in a small quantity of a hydrocarbon solvent, tetradecane ($C_{14}H_{30}$ or C14), and then added to a highly viscous polymeric solvent of polybutene (PB) (Amoco L-100, $M_w \approx 10^3$ g/mol). The final fluid composition is 0.31 wt % PIB, 4.83 wt % C14 and 94.86 wt % PB. This fluid formulation results in a viscoelastic test fluid with a moderate viscosity and high elasticity that makes it possible to attain higher values of De than was possible with the PIB/PB Boger fluids used in previous contraction flow experiments by Lawler *et al.* (1986) and Boger *et al.* (1986). The rheology of this fluid has been thoroughly characterized over a range of temperatures in linear viscoelastic, steady shear, and transient shear flow experiments (Quinzani *et al.* 1990).

The viscous and elastic characteristics of the fluid are defined in steady shear flow by the viscosity η and the first normal stress coefficient Ψ_1, and in small-amplitude oscillatory shear flow by the dynamic viscosity η' and the elastic quantity $2\eta''/\omega$ (Bird, Armstrong & Hassager 1987*a*). These material functions are shown in figure 2. The viscosity has a zero-shear-rate value $\eta_0 = 13.76$ Pa s and is almost constant over four decades of shear rate. The shear-thinning behaviour of the polymeric

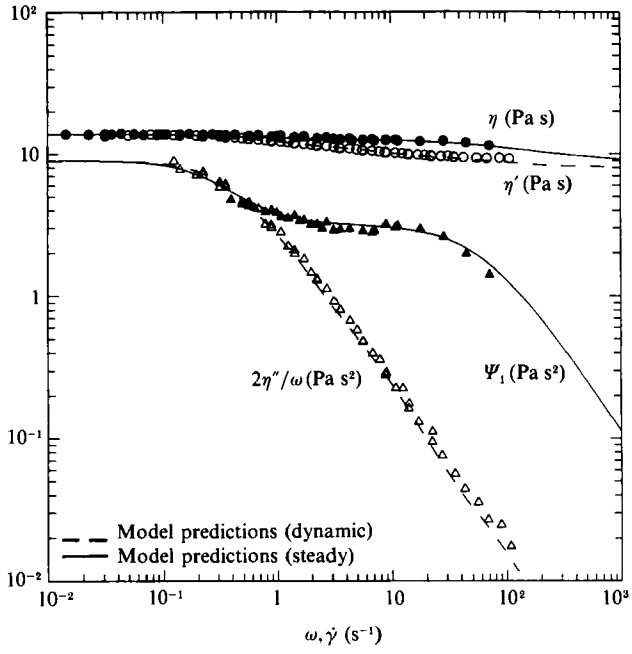

FIGURE 2. Viscous and elastic material functions for the 0.31 wt % PIB/PB/C14 test fluid at 25 °C. Solid symbols are steady-shear-flow properties: ●, viscosity η (Pa s); and ▲, first normal stress coefficient Ψ_1 (Pa s^2). Hollow symbols are linear viscoelastic properties: ○, dynamic viscosity η'; and △, $2\eta''/\omega$ (Pa s^2). Also shown are the results of fitting a four-mode Bird–DeAguiar model to the data.

contribution to the total viscosity is masked in dynamic and steady shear experiments by the presence of the highly viscous PB/C14 solvent. Quinzani *et al.* demonstrated that this solvent is Newtonian with a constant viscosity, $\eta_s = 8.12$ Pa s and makes no contribution to the elastic material functions over the shear rate and frequency ranges studied. The normal stress behaviour of the fluid is more complex, as evidenced in figure 2 by the first normal stress coefficient, $\Psi_1 (= -[\tau_{11} - \tau_{22}]/\dot{\gamma}^2)$. At very low shear rates Ψ_1 is constant, $\Psi_{10} = 8.96$ Pa s^2, indicating quadratic behaviour of the normal stresses, before the fluid begins to shear-thin at $\dot{\gamma} \approx 0.1\ s^{-1}$. At intermediate shear rates ($3 < \dot{\gamma} < 30\ s^{-1}$) the first normal stress coefficient exhibits an almost constant plateau before continuing to decrease monotonically at high shear rates. The data in figure 2 also demonstrate that in dynamic experiments the elastic quantity $2\eta''/\omega$ has the same zero-shear-rate asymptote as Ψ_1, in accordance with simple fluid theory (Bird *et al.* 1987*a*), but decreases far more rapidly at high frequencies.

Quinzani *et al.* showed that the nonlinear behaviour in the first normal stress coefficient has been measured previously in other Boger fluid systems and appears to be the result of molecular interactions between the high-molecular-weight PIB polymer chains and the polymeric (PB) solvent. Systematic experiments show that this intermediate 'plateau' region persists as the concentration of PIB in the fluid is reduced and can be observed even in a very dilute 0.01 wt % PIB/PB/C14 Boger fluid. Similar nonlinear behaviour in the first normal stress response of another thoroughly characterized Boger fluid has also been observed recently by other researchers (Laun & Hingmann 1990). The viscometric properties presented in

Mode No.	λ_k (s)	η_k (Pa s)
1	2.755	1.108
2	0.7361	1.677
3	0.1094	1.657
4	0.0098	1.211
Solvent	—	8.118

TABLE 1. Four-mode viscoelastic spectrum at 25 °C for the 0.31 wt % PIB/PB/C14 viscoelastic fluid used in these experiments (from Quinzani *et al.* 1990).

figure 2 may thus be considered as typical of highly elastic Boger fluids prepared with moderate concentrations of polyisobutylene.

The results of fitting a multimode differential constitutive equation to the experimental data are also shown in figure 2. In the past, Boger fluids have been modelled as dilute solutions of non-interacting, Hookean dumbbells in a viscous, Newtonian solvent (Prilutski *et al.* 1983; Binnington & Boger 1985). The resulting quasi-linear Oldroyd-B constitutive equation (Bird *et al.* 1987*b*) contains a single relaxation time and predicts constant viscometric properties η_0 and Ψ_{10} at all shear rates. Mackay & Boger (1987) showed that this model was inadequate for describing the transient behaviour of real Boger fluids even at moderate frequencies. To model quantitatively the rheological properties of this fluid over all frequencies and shear rates we have used a spectrum of time constants which are determined from linear viscoelasticity. A nonlinear regression technique is used to obtain the set of $\{\eta_k, \lambda_k\}$ from the dynamic viscosity η' and dynamic rigidity η'' measured in small-amplitude oscillatory shear flow. The four-mode viscoelastic spectrum obtained by Quinzani *et al.* for this Boger fluid is presented in table 1. Steady and transient nonlinear shear flow properties of the test fluid have been modelled using the relaxation spectrum in table 1 together with a multimode formulation of the Bird–DeAguiar constitutive equation (Bird & DeAguiar 1983; DeAguiar 1983), in which the PIB chains are considered to be a semi-dilute solution of finitely extensible nonlinear elastic (FENE) dumbbells. Further details of the constitutive model and its fit to rheological data for this Boger fluid are contained in Quinzani *et al.* (1990).

2.5. *Flow parameters*

The Reynolds number and Deborah number are used as scaling parameters to describe the inertial and elastic effects in the flow. A characteristic shear rate based on the downstream flow conditions is defined by $\dot{\gamma}_2 \equiv \langle v_z \rangle_2 / R_2$, where $\langle v_z \rangle_2$ is the average velocity in the small tube and R_2 is the downstream tube radius. A characteristic time for the flow is taken to be $\mathscr{T} \equiv R_2/\langle v_z \rangle_2 = \dot{\gamma}_2^{-1}$. To reflect the gradual shear thinning of the fluid elasticity at high shear rates, a shear-rate-dependent mean relaxation time $\lambda(\dot{\gamma}_2)$ is calculated from the viscometric properties of the fluid,

$$\lambda(\dot{\gamma}_2) \equiv \frac{\Psi_1(\dot{\gamma}_2)}{2\eta(\dot{\gamma}_2)}. \tag{2}$$

The relaxation time in the limit of zero shear rate is then equivalent to the relaxation time obtained from an upper convected Maxwell (UCM) constitutive model (Bird *et*

(a)

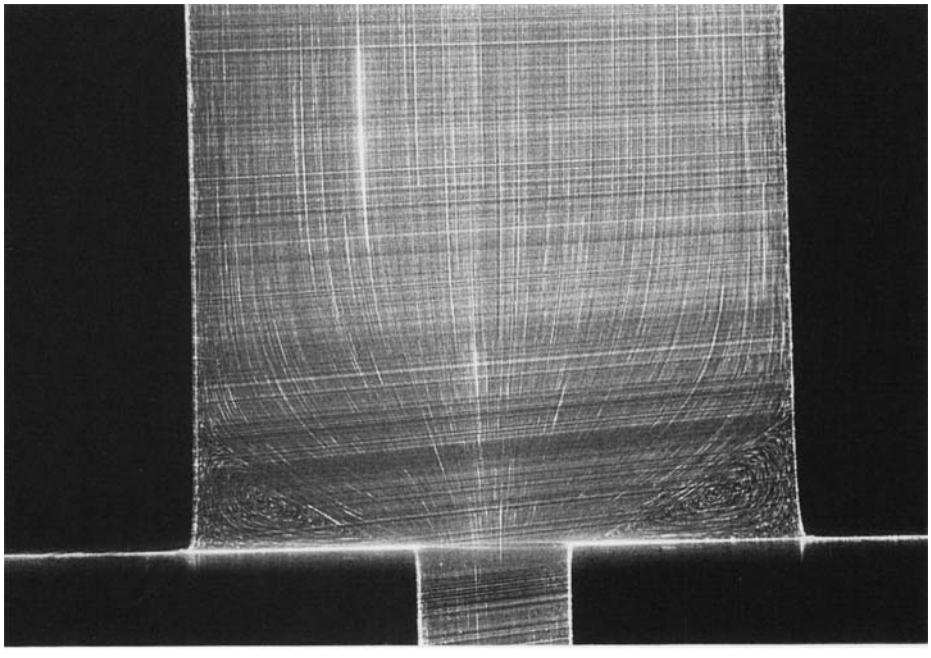

(b)

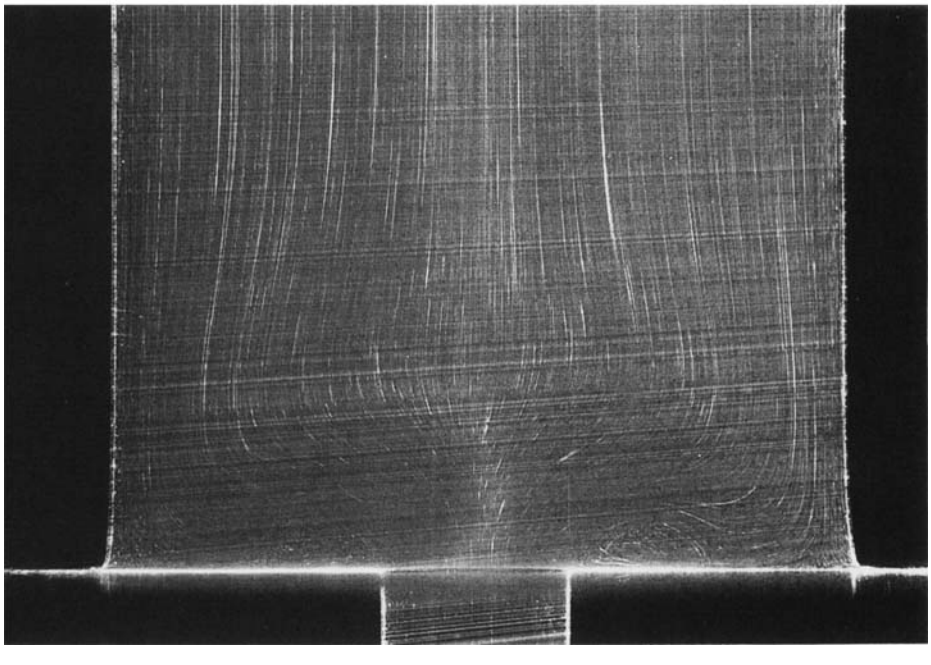

FIGURE 3(a, b). For caption see facing page.

(*c*)

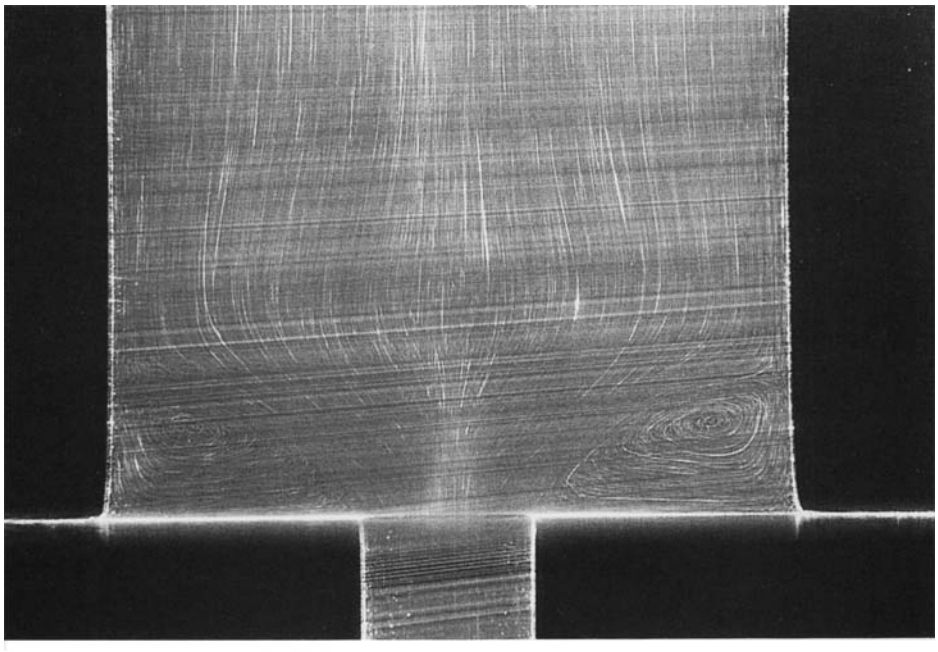

(*d*)

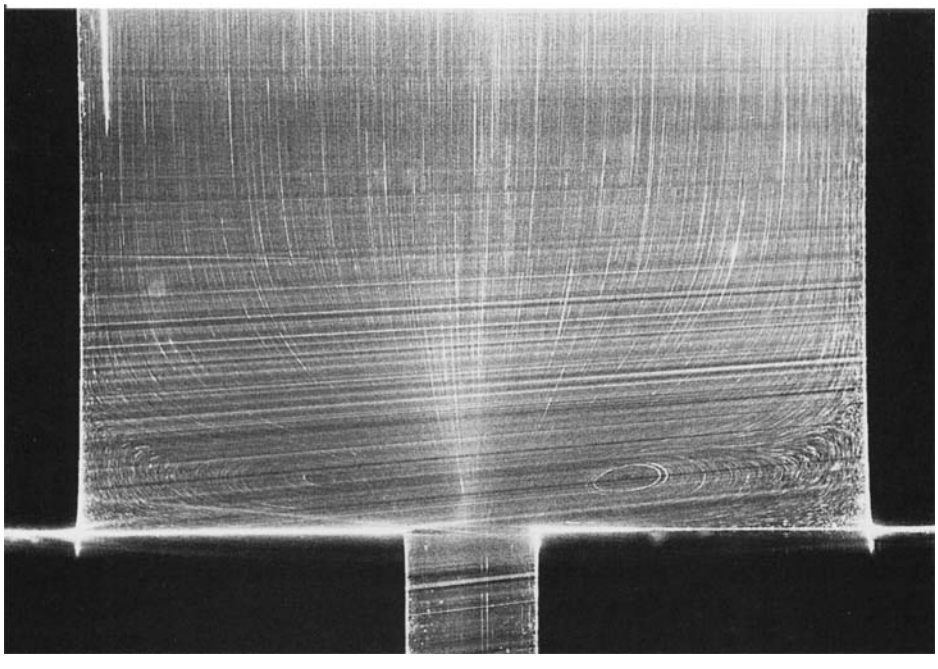

FIGURE 3. (*a–c*) Viscoelastic flow through an abrupt 4:1 axisymmetric contraction: (*a*) low flow rate with Moffat corner vortex, $De_2 = 0.90$, $Re_2 = 0.008$ (exposure time $T = 16$ s); (*b*) development of diverging streamlines and formation of lip vortex, $De_2 = 3.40$, $Re_2 = 0.041$ ($T = 8$ s); (*c*) elastic vortex growth, $De_2 = 3.92$, $Re_2 = 0.056$ ($T = 8$ s). (*d*) Coexistence of lip vortex and weak corner eddy as a single recirculation in a 6:1 axisymmetric contraction at the same flow conditions as (*b*), $De_2 = 3.40$, $Re_2 = 0.041$ ($T = 12$ s).

al. 1987*a*), $\lambda_0 = \Psi_{10}/2\eta_0 = 0.325$ s. Shear-rate-dependent Deborah and Reynolds numbers are defined respectively by

$$De_2(\dot{\gamma}_2) = \lambda(\dot{\gamma}_2)\dot{\gamma}_2, \tag{3}$$

$$Re_2(\dot{\gamma}_2) = 2\rho\langle v_z\rangle R_2/\eta(\dot{\gamma}_2). \tag{4}$$

In the current flow-loop configuration the maximum downstream shear rate achievable for the 4:1 contraction is $\dot{\gamma}_2 \approx 60\ \mathrm{s}^{-1}$ which corresponds to a Deborah number $De_2 = 4.6$ and a Reynolds number $Re_2 = 0.10$.

3. Experimental results

We first present simple flow visualization results to illustrate the structure of the transitions observed throughout the axisymmetric contraction as a function of the Deborah number. Detailed steady-state and time-dependent LDV data are then presented in §3.2 to document the sequence of nonlinear transitions that occur in the flow near the contraction lip as the Deborah number is increased. The development of a diverging flow regime and the onset of another set of dynamics associated with instability of the large elastic vortex are described in §3.3. Finally in §3.4 we show the effect of curving the lip entrance on the dynamics and flow structure observed near the lip of the 4:1 contraction.

3.1. *Flow visualization*

The macroscopic effects of elasticity on the structure of the velocity field are observed by using the flow visualization procedure described in §2.2. The streamlines observed in a 4:1 contraction at the conditions $De_2 = 0.90$ and $Re_2 = 0.008$ are shown in figure 3(*a*). At low Deborah numbers ($De_2 < 1.0$) elastic effects in the flow are negligible compared to viscous effects and the test fluid behaves as a highly viscous Newtonian liquid flowing through an abrupt axisymmetric contraction. The fluid in the upstream tube converges and accelerates directly towards the small tube. A very weak recirculation is observed in the outer corner of the large tube, as predicted by Moffatt (1964). The size of this corner vortex is characterized by a dimensionless *reattachment length* $\chi \equiv H_v/2R_1$, where H_v is the vertical height that the vortex extends upstream and R_1 is the upstream radius of the tube. Measurements from the time-exposure streak photographs at low De_2 give a value of $\chi = 0.17$ for all contraction ratios, in good agreement with the extensive experiments of Boger *et al.* (1986) and the numerical simulations of Viriyayuthakorn & Caswell (1980) and Kim-E *et al.* (1984).

As the flow rate is increased and elastic effects in the flow become important a dramatic change occurs in the shape of the streamlines. The flow field at $De_2 = 3.40$ and $Re_2 = 0.041$ is shown in figure 3(*b*). The weak corner vortex observed in Newtonian flow is greatly decreased in size and a separate intense vortex has formed at the re-entrant corner where the upstream tube joins the smaller downstream tube. The formation of this lip vortex is observed to occur in each contraction ratio at a Deborah number $De_2^{(\mathrm{lip})} > 3.0$. In addition to the formation of the lip vortex, the flow field shown in figure 3(*b*) no longer monotonically converges towards the small tube: upstream of the contraction the streamlines near the centreline diverge and fluid flows out towards the stagnant corner of the upstream tube, before rapidly accelerating into the small tube immediately above the contraction plane. This phenomenon has been documented previously in tubular entry flow experiments

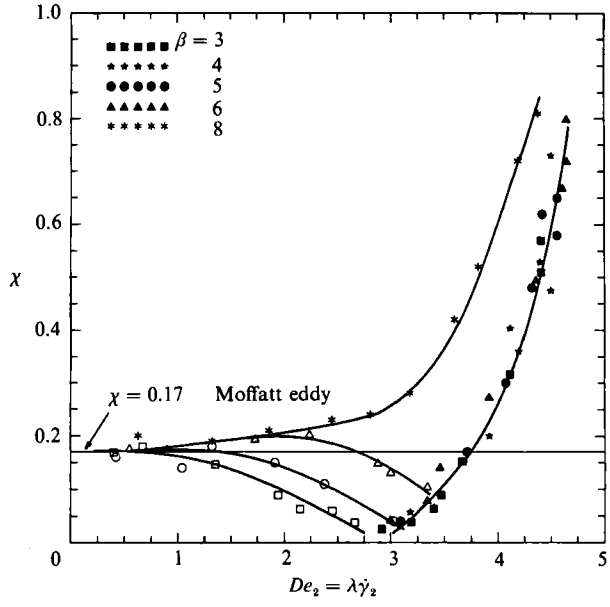

FIGURE 4. The vortex reattachment length $\chi(\equiv H_v/2R_1)$ as a function of Deborah number for each contraction ratio. The hollow symbols correspond to the Newtonian corner vortex and the solid symbols correspond to the elastic vortex which forms near the lip.

involving highly shear-thinning viscoelastic fluids at high Re (Boger & Rama Murthy 1972; Cable & Boger 1978*b*) but not in Boger fluids.

As the Deborah number is increased the elastic lip vortex increases in size and grows radially outwards towards the wall. Eventually the lip vortex fills the base of the large upstream tube and the flow enters the *vortex growth regime* in which further increases in De lead to a rapid increase in the reattachment length χ as the elastic vortex expands up the wall of the large tube. The large elastic vortex observed at $De_2 = 3.92$ and $Re_2 = 0.056$ in the 4:1 contraction is shown in figure 3(*c*). The reattachment length is determined to be $\chi = 0.21$ and continues to increase with De_2 until ultimately the flow becomes visually unstable. At $De_2 \approx 4.5$ the reattachment length is determined to be $\chi \approx 0.40$, and the vortex oscillates in size. The vortex shown in figure 3(*c*) is distinguished from the Newtonian corner vortex shown in figure 3(*a*) by its size and also by the curvature of the vortex boundary, which is concave for the Moffatt eddy at low De_2 and becomes convex for the elastic vortex at high Deborah numbers.

The variation of vortex size, as characterized by χ, with Deborah number is shown for each contraction ratio in figure 4. In the vortex growth regime at high De_2 (solid symbols) the vortex size is essentially independent of β; however, at low Deborah numbers the behaviour is more complicated. For small contraction ratios ($\beta \leqslant 5$) the size of the Newtonian corner vortex (hollow symbols) decreases from $\chi = 0.17$ as De increases until it is almost non-existent when the lip vortex forms at $De_2 = 3.0$. For higher contraction ratios ($\beta = 6$ and $\beta = 8$) the corner vortex is initially the same size, with $\chi = 0.17$ for $De_2 \ll 1$; however, it is more effectively spatially isolated from the contraction lip and does not disappear following the formation of the elastic lip vortex. Instead both vortices coexist over a range of Deborah number until the elastic vortex expands outwards from the lip and engulfs the corner vortex. The

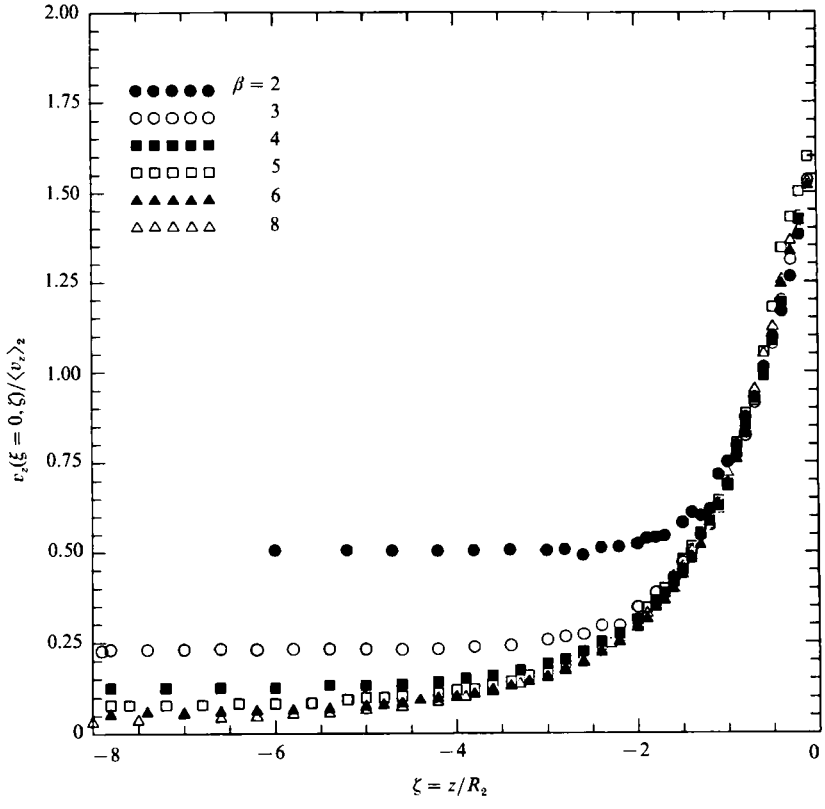

FIGURE 5. Centreline axial velocity $v_z(0, \zeta)$ in the large upstream tube for contraction ratios $2 \leqslant \beta \leqslant 8$, at flow conditions $De_2 = 0.42$, $Re_2 = 0.004$. The velocity profiles are normalized with the average downstream velocity and superimpose near the contraction $(-1 < \zeta < 0)$.

presence of both vortices is shown in figure 3(*d*) for the 6:1 contraction at $De_2 = 3.46$. This complex dependence of vortex size on contraction ratio agrees with the previous investigations of Boger *et al.* (1986) and Boger (1987).

Although macroscopic flow visualization provides a qualitative characterization of the sequence of flow transitions, from a Newtonian corner vortex to an elastic lip vortex and then to vortex growth, a far more detailed picture of the flow transitions is established by relating these global changes to LDV measurements of the local dynamics near the contraction lip and in the bulk of the flow.

3.2. *LDV measurements of flow kinematics near the lip*

3.2.1. *Newtonian flow*

The axial and radial velocity components were measured in each contraction ratio at the same volumetric flow rate of 0.32 cm^3/s, corresponding to downstream flow conditions of $De_2 = 0.42$ and $Re_2 = 0.004$. At this low De the velocity profiles correspond to a Newtonian flow. The evolution of the axial velocity along the centreline for contraction ratios $2 \leqslant \beta \leqslant 8$ is shown in figure 5. The velocity and axial position are non-dimensionalized with the downstream average velocity $\langle v_z \rangle_2$ and the tube radius R_2, respectively. Far upstream of the contraction the flow has a fully developed parabolic profile, and the centreline velocity for each contraction ratio is $v_z/\langle v_z \rangle_2 \equiv 2/\beta^2$. As the fluid approaches the contraction plane the flow

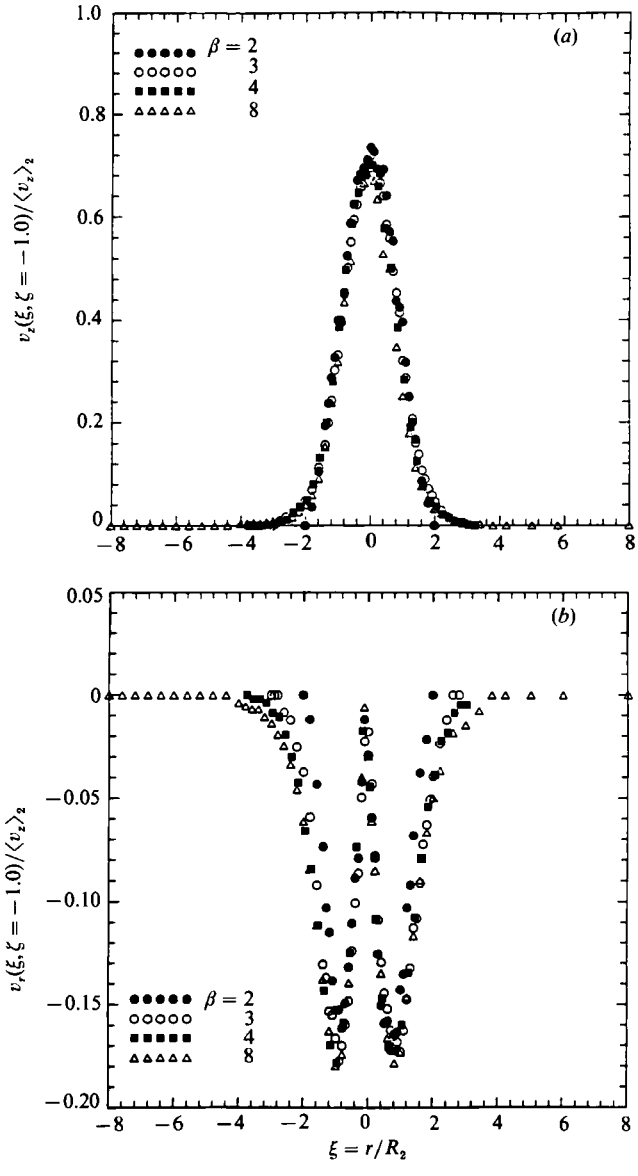

FIGURE 6. Axial velocity profiles $v_z(\xi, -1)$ and (*b*) radial velocity profiles $v_r(\xi, -1)$ above the contraction plane at a low Deborah number, $De_2 = 0.42$, and $Re_2 = 0.04$ for contraction ratios of $\beta = 2$, 3, 4 and 8. The profiles superimpose when scaled with the downstream parameters R_2 and $\langle v_z \rangle_2$.

accelerates into the small tube and the data for each contraction ratio superimpose. Downstream of the contraction the flow again assumes a fully developed parabolic profile with centreline velocity $v_z/\langle v_z \rangle_2 \equiv 2$. Radial profiles of the axial and radial velocity components at $\zeta = -1.0$ are shown in figures 6(*a*) and 6(*b*) respectively. The profiles again superimpose when the velocity and position are scaled with the downstream tube conditions, except near the outer walls of the upstream tube. These results indicate that the Newtonian flow near the contraction plane is governed by conditions in the small tube and is relatively independent of the contraction ratio, β.

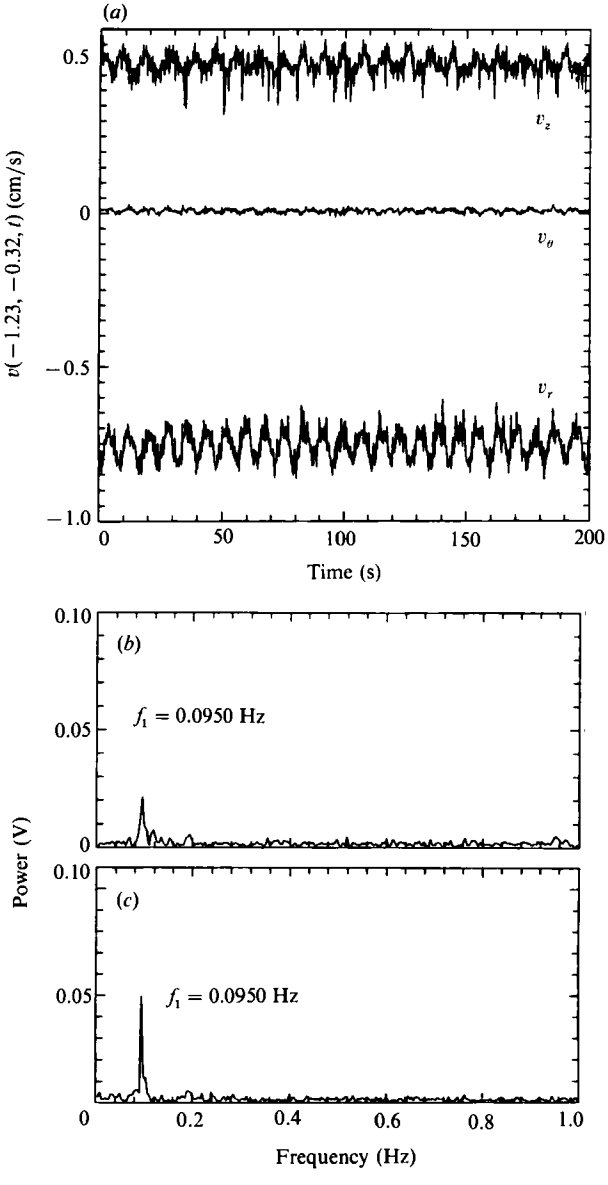

FIGURE 7. (*a*) Sample time series data showing oscillations of all three velocity components near the lip ($\xi = -1.23, \zeta = -0.32$) of the 4:1 contraction at $De_2 = 1.70$, $Re_2 = 0.015$. (*b*) Frequency spectrum of the axial velocity component in (*a*); the frequency of oscillation is $f_1 = 0.0950$ Hz. (*c*) Frequency spectrum of the radial velocity component in (*a*); the frequency of oscillation is $f_1 = 0.0950$ Hz.

This scaling has also been documented by Raiford *et al.* (1989) for axisymmetric contraction flows of a highly shear-thinning solution of 5 wt % polyisobutylene in tetradecane.

3.2.2. *The lip instability*: $2 \leqslant \beta \leqslant 5$

For moderately low Deborah numbers ($De_2 \leqslant 1.5$) the velocity components near the lip remain steady and two-dimensional as the flow rate through the 4:1

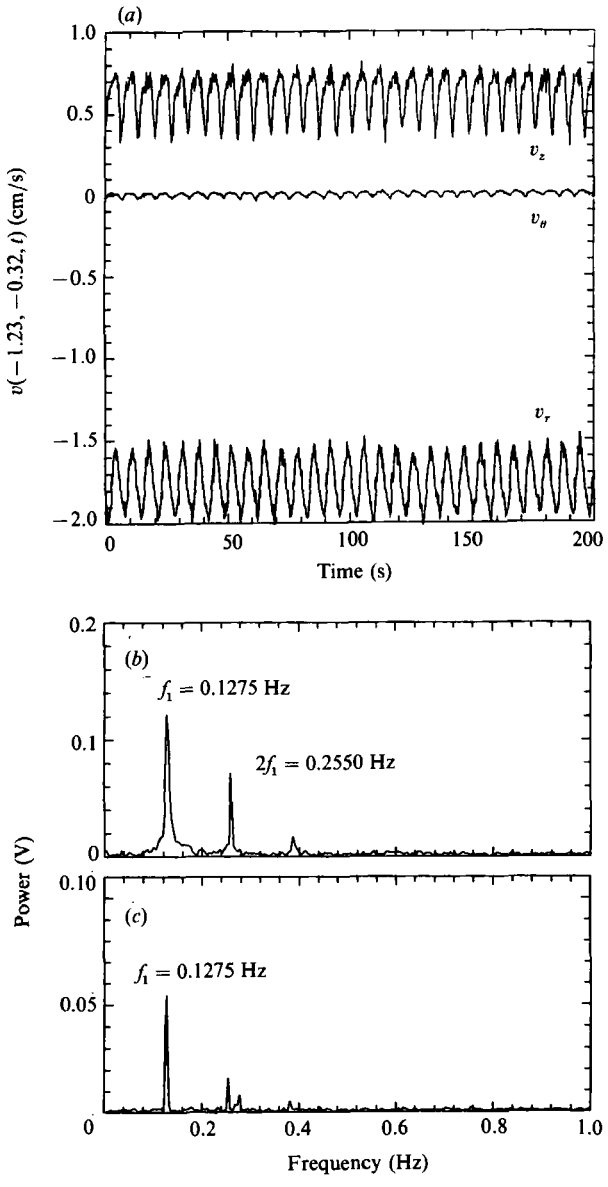

FIGURE 8. (*a*) Sample time series data showing increased amplitude of oscillations in all three velocity components near the lip ($\xi = -1.23, \zeta = -0.32$) of the 4:1 contraction at $De_2 = 2.12$, $Re_2 = 0.016$. (*b*) FFT frequency spectrum of the axial velocity component in (*a*); the frequency of oscillation is $f_1 = 0.1275$ Hz. (*c*) FFT spectrum of the tangential velocity component in (*a*); the frequency of oscillation is $f_1 = 0.1275$ Hz.

contraction is increased. At a critical Deborah number $De_2^{(osc)} \approx 1.5$ the flow near the lip undergoes a Hopf bifurcation to a three-dimensional, time-dependent motion and oscillations develop in the axial, radial, and tangential velocity components. These velocity fluctuations are small in amplitude and are localized to the lip region upstream of the contraction plane ($-1.5 \leqslant \xi \leqslant 1.5, -1.5 \leqslant \zeta \leqslant 0$). LDV measurements further upstream and downstream of the contraction plane remain steady. It is emphasized that the flow visualization 'streak' photographs result in a time-

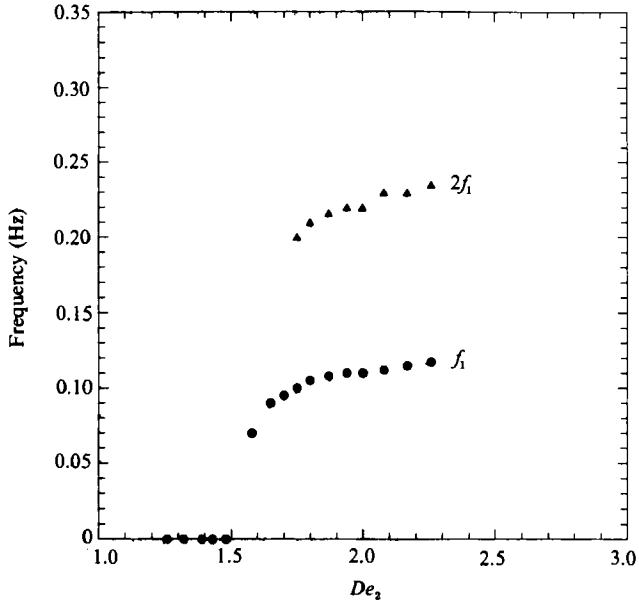

FIGURE 9. Frequency of oscillations in the axial velocity near the lip of the 4:1 contraction ($\xi = 1.15, \zeta = -0.30$) as a function of the Deborah number.

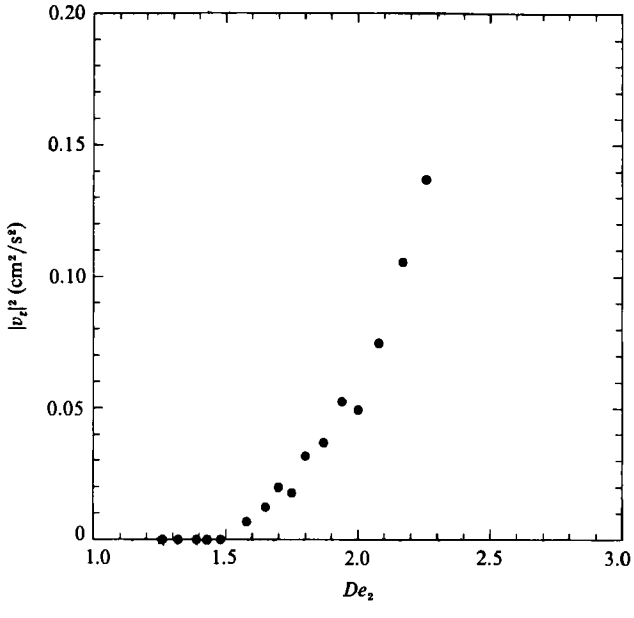

FIGURE 10. Square of the amplitude of oscillations in v_z near the lip of the 4:1 contraction ($\xi = 1.15, \zeta = -0.30$) as a function of the Deborah number.

averaged picture of the flow field and do not indicate any change to the overall flow pattern. These time-periodic oscillations are followed by using the trackers; sample time series for the axial, radial and tangential velocity components near the lip are shown in figures 7 and 8. The time-dependent tangential velocity component v_θ that develops is observed to oscillate about a zero mean, as first observed by Lawler *et al.*

β	Q (cm^3/s)	$\dot{\gamma}_2$ (s^{-1})	$\lambda(\dot{\gamma}_2)$ (s)	De_2	Re_2	τ_w (kPa)	N_{1w} (kPa)	$\frac{N_{1w}}{\tau_w}$
2	1.59	15.85	0.141	2.04	0.022	0.747	7.486	10.02
3	1.23	12.19	0.147	1.79	0.017	0.583	5.062	8.68
4	1.01	10.08	0.149	1.50	0.014	0.490	3.754	7.66
5	1.62	16.10	0.140	2.27	0.022	0.759	7.724	10.18

TABLE 2. Flow parameters at the formation of a time-dependent lip vortex for contraction ratios $\beta = 2$, 3, 4 and 5. The subscript '2' denotes rheological properties evaluated at the average flow conditions in the downstream tube. The subscript 'w' indicates the rheological properties are calculated at the wall shear rate in the downstream tube where $\dot{\gamma}_w = 4\dot{\gamma}_2$. The stress ratio is defined as $N_1/\tau \equiv \Psi_1(\dot{\gamma})\dot{\gamma}/\eta(\dot{\gamma})$ and is evaluated at the downstream wall shear rate.

(1986). The frequency of oscillation in each component is calculated by performing a fast Fourier transform (FFT) of the velocity data. The initial frequency of oscillation for each component in the 4:1 contraction is determined from the FFTs in figures 7(*b*) and 7(*c*) to be $f_1 = 0.0950$ Hz. As the Deborah number is increased these velocity fluctuations grow in amplitude, the frequency of oscillation increases, and harmonics of the fundamental frequency appear in the FFT spectrum, as shown in figures 8(*b*) and 8(*c*).

The variation of oscillation frequency determined from FFT spectra, such as those in figures 7 and 8, is summarized in figure 9 as a function of Deborah number for $\beta = 4$. In addition the square of the oscillation amplitude in v_z near the lip as a function of the Deborah number is shown in figure 10. The critical Deborah number for onset of periodic flow is determined accurately by fitting these data to the results of an asymptotic analysis for a supercritical Hopf bifurcation (Iooss & Joseph 1980) which predicts that the amplitude of oscillation should be of the form

$$|v(r, \theta, z, t)| \propto (De - De^{(\mathrm{osc})})^{\frac{1}{2}} e^{i\omega t}. \tag{5}$$

Near the onset point the data are linear in agreement with equation (5), and extrapolation to $|v_z| = 0$ determines the critical value of De to be $De_2^{(\mathrm{osc})} = 1.50 \pm 0.02$. The large nonlinear increase in amplitude at higher De results from the introduction of harmonics of the fundamental oscillation frequency.

A similar Hopf bifurcation in a 4:1 axisymmetric contraction was first observed by Lawler *et al.* (1986) for a less elastic PIB/PB/K Boger fluid. In sharp contrast to the results described here, they observed the flow to return to a two-dimensional steady state as the Deborah number was increased. With the PIB/PB/C14 fluid used here the flow remains time-dependent for all Deborah numbers greater than $De_2^{(\mathrm{osc})}$ and subsequently undergoes a series of nonlinear transitions.

Experiments in other contraction ratios indicate that the local dynamics of the flow transition are highly sensitive to the contraction ratio. The onset of time-periodic flows was detected for contraction ratios $2 \leqslant \beta \leqslant 5$. The flow conditions and critical Deborah number $De_2^{(\mathrm{osc})}$ at onset of oscillations are listed in table 2. The value of $De_2^{(\mathrm{osc})}$ displays a minimum at $\beta = 4$ and increases for both larger and smaller contraction ratios. The frequencies of oscillation near the lip for $\beta = 3$, 4 and 5 are shown in figure 11. The critical Deborah numbers of the Hopf bifurcation are determined from the plots of the square of the oscillation amplitude shown in figure 12 to be $De_2^{(\mathrm{osc})} = 1.71$ and 2.20 for $\beta = 3$ and 5, respectively. Again the oscillations developed in all three velocity components and remained localized to the lip region.

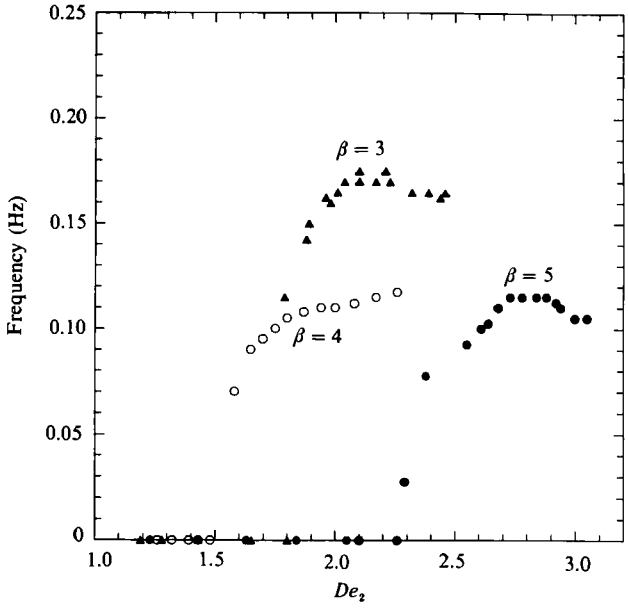

FIGURE 11. Frequency of oscillations in the radial velocity near the lip as a function of the Deborah number for $\beta = 3$, 4 and 5.

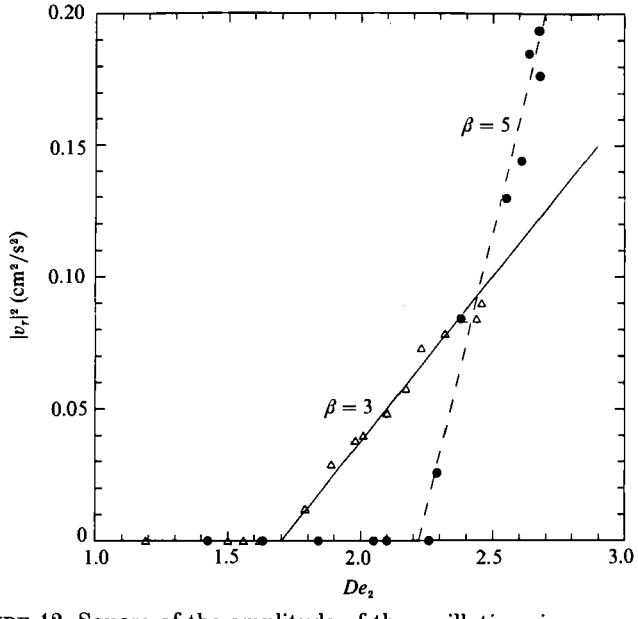

FIGURE 12. Square of the amplitude of the oscillations in v_r near the lip as a function of the Deborah number for $\beta = 3$ and 5.

The flow appeared steady away from the lip with no visual changes to the global structure. Experiments in the 2:1 contraction showed a similar transition to time-periodic flow at $De_2 = 2.04$. No Hopf bifurcation was detected in experiments with contraction ratios of $\beta = 6$ and 8 up to a critical Deborah number where the large-scale vortex dynamics described in §3.3.2 became dominant.

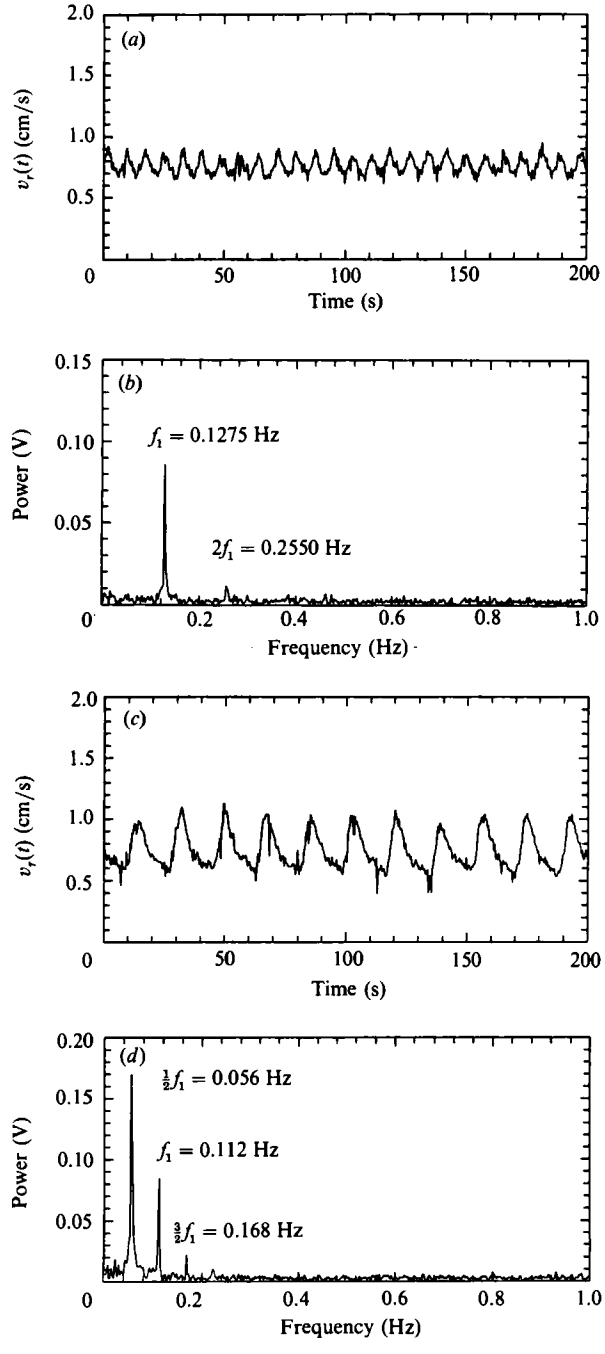

FIGURE 13. Time series data showing period doubling of the oscillations in the radial velocity component near the lip ($\xi = 1.68, \zeta = -0.30$) of the 4:1 contraction. The time series (*a*) at $De_2 = 2.55$ ($Re_2 = 0.026$) has small-amplitude oscillations, and the fundamental frequency (*b*) before period doubling is $f_1 = 0.1275$ Hz. After the period-doubling transition the time series (*c*) at $De_2 = 2.62$ ($Re_2 = 0.027$) shows larger oscillations, and the FFT spectrum (*d*) contains additional spectral peaks at $\frac{1}{2}f_1$ and $\frac{3}{2}f_1$.

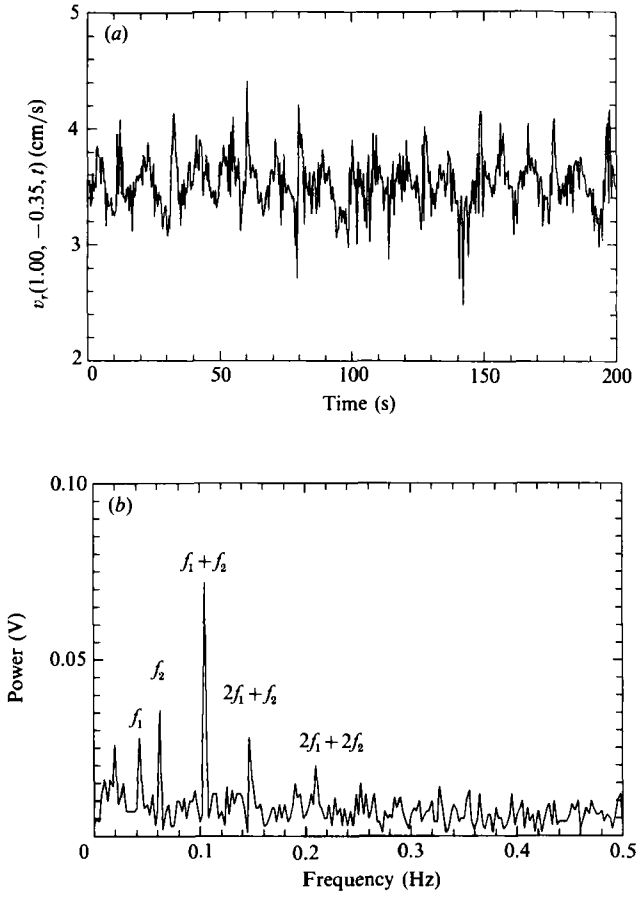

FIGURE 14. Time series and frequency spectrum showing quasi-periodic oscillations in the velocity near the lip of the 5:1 contraction ($\xi = 1.00, \zeta = -0.5$) at $De_2 = 3.09$, $Re_2 = 0.034$: (*a*) radial velocity profile as a function of time; (*b*) FFT spectrum, $f_1 = 0.043$ Hz, $f_2 = 0.063$ Hz.

3.2.3. *Period-doubling transition*: $3 \leqslant \beta \leqslant 5$

As the Deborah number is increased the amplitude of the oscillations in the velocity components grows, and higher harmonics of the oscillation frequency $2f_1$, $3f_1$ appear in the frequency spectrum. A subharmonic period-doubling instability is observed in the 4:1 contraction at $De_2 = 2.60$. This transition results in a large increase in the oscillation amplitude and a spectral peak at $\frac{1}{2}f_1$ which grows rapidly in strength to dominate the frequency spectrum. These effects are demonstrated by comparing the two sets of time-series and frequency spectra presented in figure 13 for the radial velocity component near the lip ($\xi = 1.68, \zeta = -0.30$) of the 4:1 contraction. The frequency of oscillation shown in figure 13(*d*) following the period-doubling transition is 0.065 Hz. A similar period-doubling transition is also observed for $\beta = 3$ and $\beta = 5$ at Deborah numbers $De_2 > 2.5$. Further increases in De_2 however did not result in subsequent period-doubling transitions and the appearance of $\frac{1}{4}f_1$ peaks in the frequency spectrum. Instead, another Hopf bifurcation is observed in the flow at $De_2 = 3.0$ resulting in a quasi-periodic flow state.

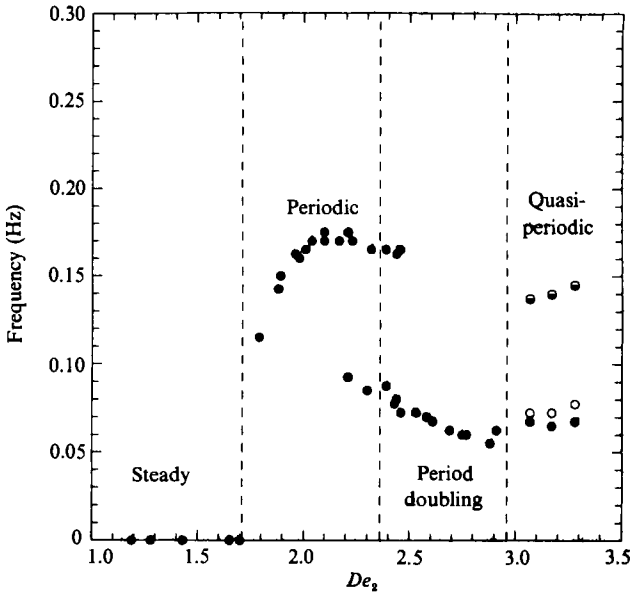

FIGURE 15. Dominant frequencies in the time-dependent regimes near the lip of the 3:1 contraction as a function of the Deborah number. In the quasi-periodic regime the three strongest peaks in the FFT spectrum are identified as: ●, f_1; ○, f_2; ◒, f_1+f_2.

3.2.4. *Quasi-periodic flow near the lip*: $2 \leqslant \beta \leqslant 5$

Quasi-periodic flow regimes characterized by two independent frequencies were observed in the contraction ratios $2 \leqslant \beta \leqslant 5$ for $De_2 > 3.0$. The frequency spectrum shown in figure 14 for flow in a 5:1 contraction consists of two distinct oscillation frequencies (f_1,f_2) and a number of other peaks which can be identified as linear combinations of the form $m_1 f_1 + m_2 f_2$, where m_1 and m_2 are integers. The two fundamental frequencies are determined from figure 14 to be $f_1 = 0.043$ Hz and $f_2 = 0.063$ Hz within the limits of spectral resolution attainable with the current experimental apparatus. The evolution of the dominant frequencies in the 3:1 contraction from $De_2 = 1.0$–3.5 is summarized in figure 15.

The development of a quasi-periodic state from a time-periodic regime was approximately independent of contraction ratio for $2 \leqslant \beta \leqslant 5$ and occurred in each contraction ratio at a Deborah number $De_2^{(\mathrm{lip})} \approx 3.0$. At this Deborah number the flow visualization results presented in figure 3(*b*) show a distinct change in the flow field and the formation of an intense *lip vortex* in the same spatial region where quasi-periodic time-dependence is observed. Analysis of the videotape also shows that this vortex oscillates in size. LDV results for the higher contraction ratios $\beta = 6$ and 8 indicate that the flow is not time-dependent at $De_2 = 3.0$; however, the formation of a steady lip vortex is still observed in streak photographs such as figure 3(*d*) and can be measured quantitatively by using the LDV system. Figure 16 shows the radial and axial velocity components in the 6:1 contraction near the lip ($\xi = -1.50$, $\zeta = -0.30$) as a function of Deborah number. Initially, the magnitudes of both velocity components increase and the radial velocity is negative indicating inward flow towards the throat. At a Deborah number of 2.96 the axial velocity decreases, and the radial velocity reverses in direction as the lip vortex forms and the fluid near the contraction lip flows outwards into the corners of the large tube.

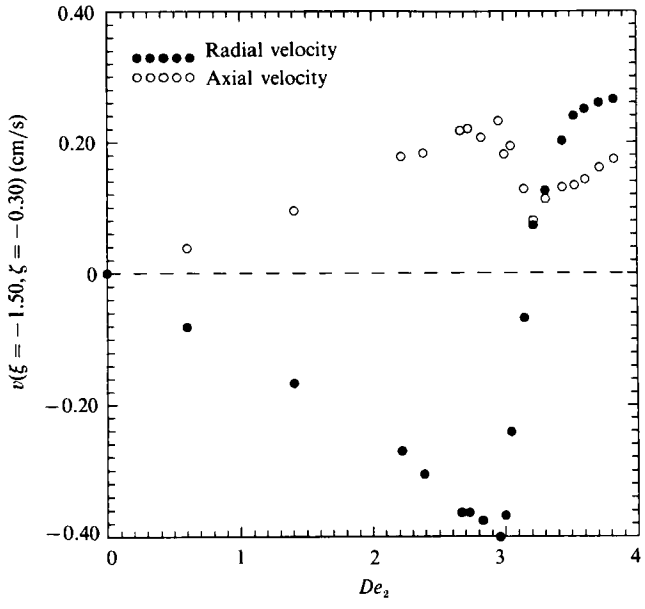

FIGURE 16. Steady-state radial and axial velocity profiles as functions of Deborah number near the lip of the 6:1 contraction ($\xi = -1.50, \zeta = -0.30$). The formation of a lip vortex at $De_2 = 2.96$ is clearly identified by the reversal in flow direction of the radial velocity component.

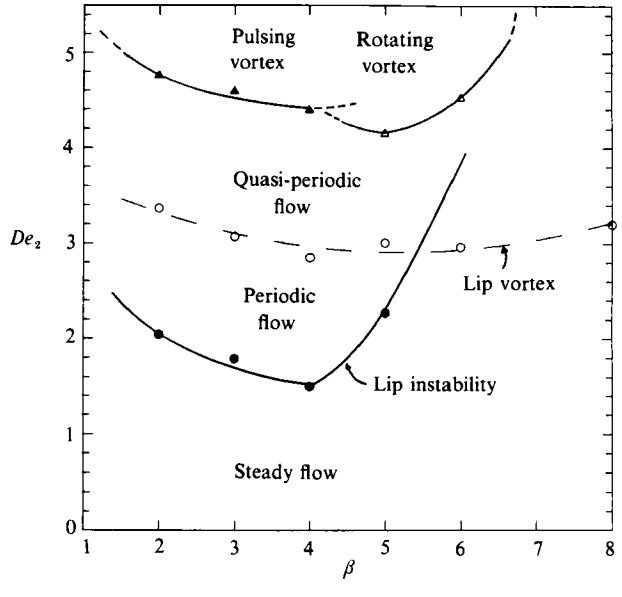

FIGURE 17. Flow transitions in the axisymmetric abrupt contraction as functions of the contraction ratio for $2 \leqslant \beta \leqslant 8$: ●, the critical Deborah number $De_2^{(osc)}$ for Hopf bifurcation to a time-dependent flow regime near the lip; ○, the critical Deborah number $De_2^{(lip)}$ for the formation of a lip vortex. At higher Deborah numbers the large elastic vortex present in the upstream tube becomes unstable to either a pulsing (▲) or rotating (△) flow.

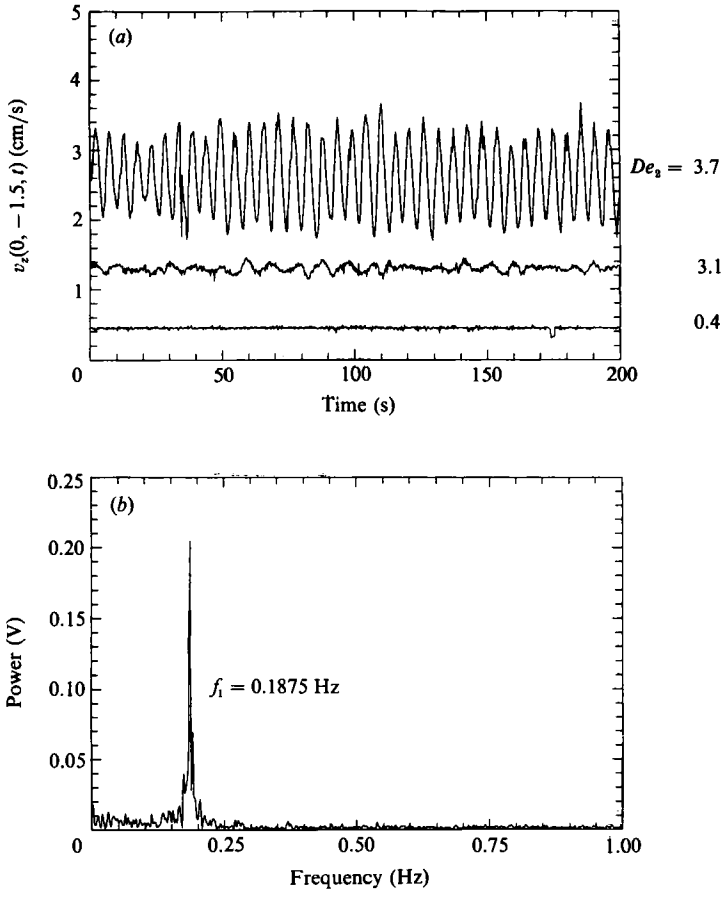

FIGURE 18. (*a*) Time series of the axial velocity on the centreline ($\xi = 0, \zeta = -1.50$), $Re_2 = 0.05$, of the 4:1 contraction at $De_2 = 0.4$, 3.1, 3.7; (*b*) FFT spectrum of the time-dependent axial velocity shown in (*a*) at $De_2 = 3.7$.

The complex dependence of the steady and time-dependent flow dynamics on contraction ratio is represented graphically by the stability diagram shown in figure 17. The critical Deborah numbers for development of time-periodic flow near the lip, $De_2^{(osc)}$, and for the formation of a lip vortex, $De_2^{(lip)}$, are shown as functions of contraction ratio. These flow transitions are considered to be two separate, competing modes of elastic phenomena. For moderate contraction ratios $2 \leqslant \beta \leqslant 5$ the most unstable mode, i.e. the instability occurring at lowest De_2, leads to a time-periodic flow regime near the lip, which is followed by development of a quasi-periodic lip vortex. However, for the larger contraction ratios $\beta = 6$ and 8, the formation of a steady lip vortex (which coexists with the corner vortex) occurs first.

Increasing the Deborah number beyond $De_2^{(lip)}$ resulted in growth of the lip vortex vertically upstream and radially outwards until at $De_2 = 3.8$ the recirculation in the 4:1 contraction covered the base of the large upstream tube. The increasing size of the lip vortex was accompanied by an expansion in the spatial extent of the time-dependent flow and an increase in the amplitude of the velocity oscillations. Sample time series of the axial velocity on the centreline near the lip of the 4:1 contraction as the Deborah number was increased are shown in figure 18. At low De_2 the flow field

is Newtonian, and the velocity is steady throughout the upstream and downstream tubes. At $De_2 = 3.10$ a small time-dependent lip vortex has formed near the lip, and velocity data measured within the lip vortex indicate a quasi-periodic flow, as typified by figure 15(*a*). The axial velocity on the centreline near the lip ($\zeta = -1.50$) now contains small fluctuations about its average value; however, an FFT of the time series at $De_2 = 3.10$ shown in figure 18(*a*) revealed no dominant frequency of oscillation. At $De_2 = 3.70$ the lip vortex has grown substantially in size ($\chi = 0.12$) and almost extends across the entire width of the upstream tube. Oscillations in the velocity field extend spatially throughout the throat region and the axial velocity on the centreline shows large-amplitude, time-dependent fluctuations. LDV measurements in the lip region at this Deborah number show quasi-periodic behaviour; however, farther from the re-entrant corner the velocity field is affected predominantly by the large-amplitude fluctuations in the size of the lip vortex, and velocity measurements on the centreline indicate essentially a time-periodic behaviour as shown in figure 18(*a*). The dominant frequency of oscillation was determined from the Fourier spectrum in figure 18(*b*) to be $f = 0.1875$ Hz. Farther upstream from the lip the flow remains steady, and LDV measurements at $\zeta = -5.0$ and -10.0 showed no time-dependent behaviour.

3.2.5. *Aperiodic flow*: $3 \leqslant \beta \leqslant 5$

Upon reaching the corners of the upstream tube the lip vortex grew rapidly to form the large convex elastic vortex shown in figure 3(*c*) and the time-dependent nature of the flow underwent a third transition. Experimental time series no longer exhibited clear quasi-periodic oscillations; instead aperiodic fluctuations in the velocity components were observed with no well-resolved spectral peaks. This behaviour is demonstrated in figure 19(*a*) by the axial velocity on the centreline at $\zeta = -2.25$ in the 4:1 contraction. The Deborah number is $De_2 = 4.08$, and the lip vortex has expanded upstream to a height of $\chi = 0.21$. The time series shows both slow and rapid fluctuations in magnitude. The FFT spectrum in figure 19(*b*) contains broadband noise across the spectrum with no dominant oscillation frequency. By replotting the data on a logarithmic scale, the level of noise measured in this frequency spectrum is shown to be significantly increased above the instrumental 'white' noise that is observed in the FFT spectra previously presented in the periodic and quasi-periodic flow regimes, particularly in the very low (<0.2 Hz)-frequency range. The signal-to-noise resolution of the LDV photomultipliers and the limited time window of observation possible with this open-flow system prevent the extremely long data runs necessary to quantify a chaotic flow regime in detail (Gollub & Benson 1980; Bergé, Pomeau & Vidal 1986). However, it is clear that upon entering the vortex growth regime the flow dynamics becomes more complex than the quasi-periodic flow observed at lower values of the Deborah number. These velocity fluctuations near the lip persisted as the Deborah number was increased and as the elastic vortex increased in size. Similar FFT spectra were observed for $\beta = 3$ and 5; however, no data could be obtained in the 2:1 contraction since the frequency trackers were unable to follow the LDV signal. In the large contraction ratios ($\beta = 6$ and 8) the flow near the lip remained steady as the Deborah number was increased, until the onset of the global vortex instability to be described in §3.3.2.

Two previous experimental investigations of flow through 4:1 contractions have used similar PIB/PB Boger fluids: Lawler *et al.* (1986) observed that the time-dependent flow near the lip reverted to steady two-dimensional flow at a second critical Deborah number, and Boger (1987) reported that the time-dependent lip

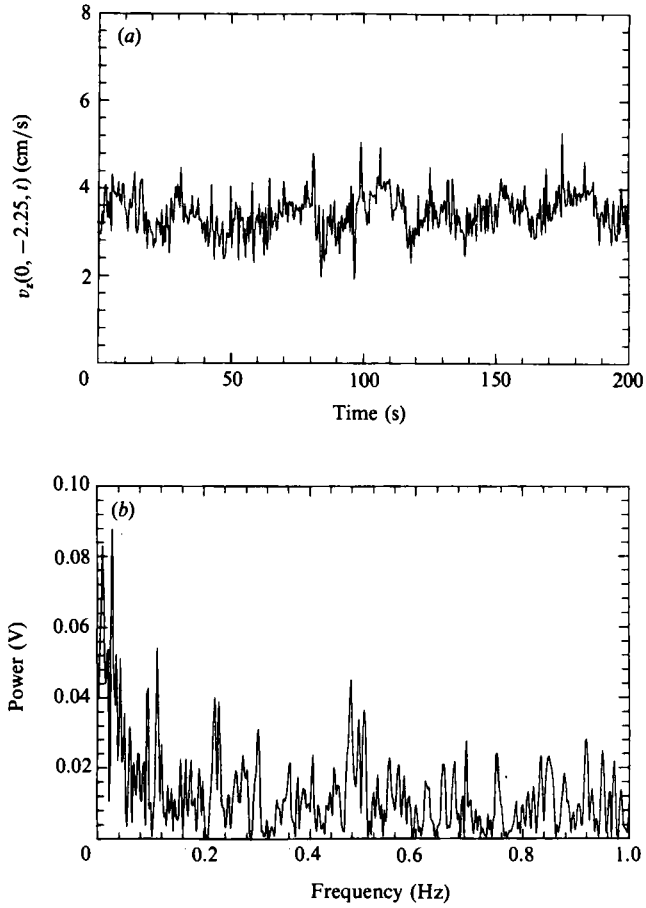

FIGURE 19. Aperiodic flow along the centreline near the lip ($\xi = 0, \zeta = -2.25$) of the 4:1 contraction at $De_2 = 4.08$ and $Re_2 = 0.061$. The axial velocity (*a*) shows random fluctuations and the FFT (*b*) has no fundamental frequency of oscillation, but contains broadband noise across the entire spectrum.

vortex observed qualitatively at low De was followed by a steady two-dimensional vortex growth regime. However, in our experiments the flow in the low contraction ratios ($\beta \leqslant 5$) remains time-dependent for all De_2 above the critical Deborah number, $De_2^{(\mathrm{osc})}$. The reason for this difference is still unclear but must be related to differences in the rheology of the test fluids. The aperiodic oscillations in the velocity occur over the same range of values of β and De_2 for which diverging streamlines upstream of the contraction are observed (see figure 3*c*). This diverging flow regime is documented in more detail in §3.3.1 and did not occur in the previous investigations with PIB/PB fluids. These velocity fluctuations may thus result from a time-dependent instability connected with the development of a diverging flow structure upstream of the contraction plane.

3.3. *Global kinematic changes*

In addition to the development of localized time-dependent flow near the contraction lip, increasing the Deborah number results in modifications of the flow structure throughout the axisymmetric contraction. These phenomena are described in this section.

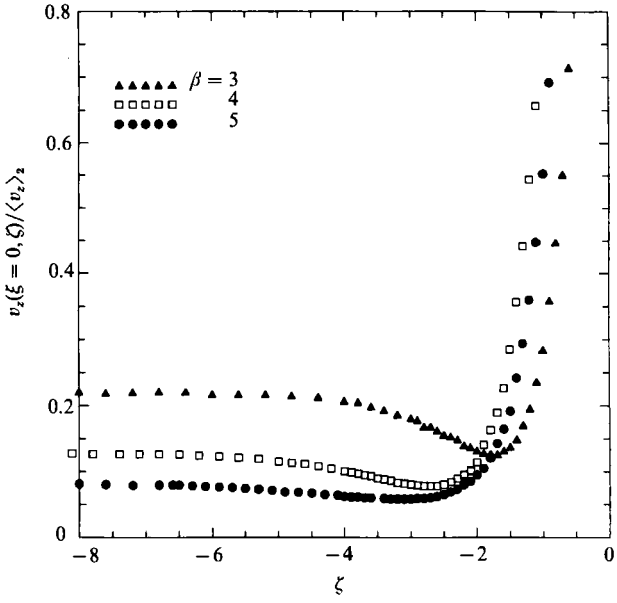

FIGURE 20. Diverging flow upstream of the contraction plane at high De_2 demonstrated by the normalized axial velocity $v_z(0, \zeta)/\langle v_z \rangle_2$ along the centreline for contraction ratios $\beta = 3$, 4 and 5, $De_2 = 3.7$, 3.9 and 3.7 respectively.

3.3.1. *Diverging flow regime*: $2 \leqslant \beta \leqslant 5$

At high Deborah numbers the flow upstream of the contraction plane becomes *divergent* and the fluid upstream of the contraction plane moves radially outwards away from the centreline; this phenomenon is demonstrated in figure 3(*b*, *c*). An increase in the velocity away from the centreline must result in a reduced axial velocity along the centreline to conserve mass flow across each plane throughout the upstream tube. Time-averaged LDV measurements of the axial velocity component along the centreline in the upstream tube are shown in figure 20 for $\beta = 3$, 4 and 5. Far upstream the velocity profile remains parabolic and the normalized centreline axial velocity is $\langle v_z \rangle_2 \equiv 2/\beta^2$, in agreement with figure 5. As the fluid approaches the contraction throat it does not accelerate monotonically but initially decelerates and the velocity reaches a local minimum at $\zeta \approx -2.0$. Closer to the contraction plane the velocity increases rapidly. Transverse profiles of the axial velocity at $\zeta = -3.0$ for contraction ratios $\beta = 3$, 4 and 5 are shown in figure 21. The profiles are no longer parabolic but show maxima away from the centreline. Subsequent increases in the Deborah number do not diminish this divergent effect but result in an increase in the size of the elastic vortex which exists at these flow rates and an associated shift upstream in the position of the velocity minimum as shown in figure 3(*b*, *c*).

As seen in figure 21, the magnitude of the deceleration associated with the diverging flow is strongly dependent on the contraction ratio, with the largest decreases in velocity occurring in the smaller contraction ratios. No velocity minima were observed at any experimentally attainable Deborah number in the larger contraction ratios ($\beta = 6$ and 8), and the flow accelerated monotonically towards the throat. Although this elastic phenomenon first develops at Deborah numbers comparable with those at which the lip vortex forms it does not appear that the two effects are directly related, since the diverging flow persists into the vortex growth

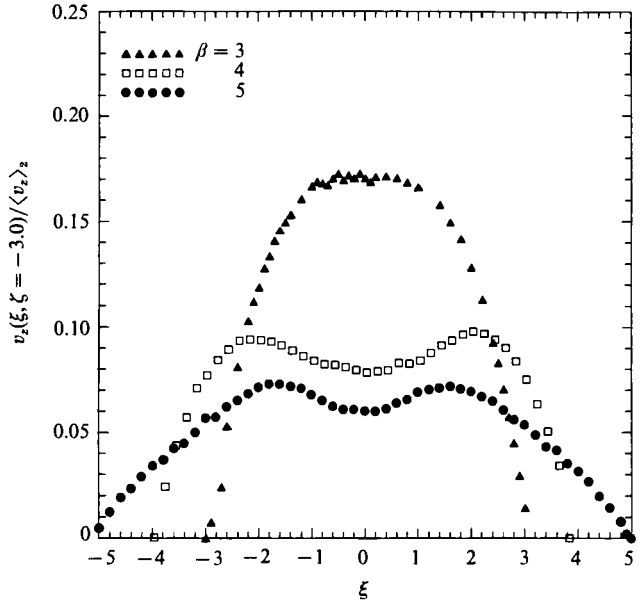

FIGURE 21. Transverse axial velocity profiles $v_z(\xi)/\langle v_z \rangle_2$ at $\zeta = -3.00$ for contraction ratios $\beta = 3$, 4 and 5 at the same De_2 as shown in figure 20. The profiles show pronounced off-centreline maxima which vary with contraction ratio.

regime (see figure 3*c*). In addition, lip vortices have been reported in Boger fluids with no associated diverging flow (Boger *et al.* 1986) whereas a diverging flow regime has been observed in shear-thinning fluids with no lip vortex formation (Cable & Boger 1978*a*; Evans & Walters 1989). This is the first time that this phenomenon has been documented in axisymmetric contraction flow of a Boger fluid, although diverging streamlines have been observed by Binding & Walters (1988) in the flow of a PAC/CS Boger fluid through a 4:1 planar contraction.

The sensitive dependence of the diverging flow on contraction ratio indicates that flow conditions in the upstream tube play an important role in the sequence of viscoelastic flow transitions. In steady simple shearing flows a gradual shear thinning is observed in viscometric properties such as η and Ψ_1. However, in uniaxial extensional flows, such as that along the centreline of an axisymmetric contraction, Boger fluids extensionally thicken and exhibit an elongational viscosity much greater than the viscosity measured in steady shear flow. The data for each contraction ratio shown in figure 20 show that the maximum extension rate experienced along the centreline, $\dot{\epsilon} = \partial v_z/\partial z$, is almost the same for $\beta = 3$, 4 and 5. Thus the same degree of extensional thickening is expected in each contraction ratio, and the extensional viscosity behaviour of Boger fluids alone cannot be used to directly differentiate between the results in each contraction. However, for the same downstream flow conditions De_2 (and hence the same $\dot{\gamma}_2$), the average upstream shear rate $\dot{\gamma}_1$ is given by $\dot{\gamma}_2/\beta^3$, and therefore differs greatly in each contraction. In addition the shear rate varies linearly across the upstream tube and reaches a maximum $\dot{\gamma}_{1w} = 4\dot{\gamma}_1$ at the wall. The maximum shear rate in the upstream tube and the greatest shear thinning in the fluid properties is experienced near the wall of the 3:1 contraction. In §4 we suggest that this variation in the upstream shear rate and the dependence of the total Hencky strain on β may be important in explaining the appearance of the diverging flow field.

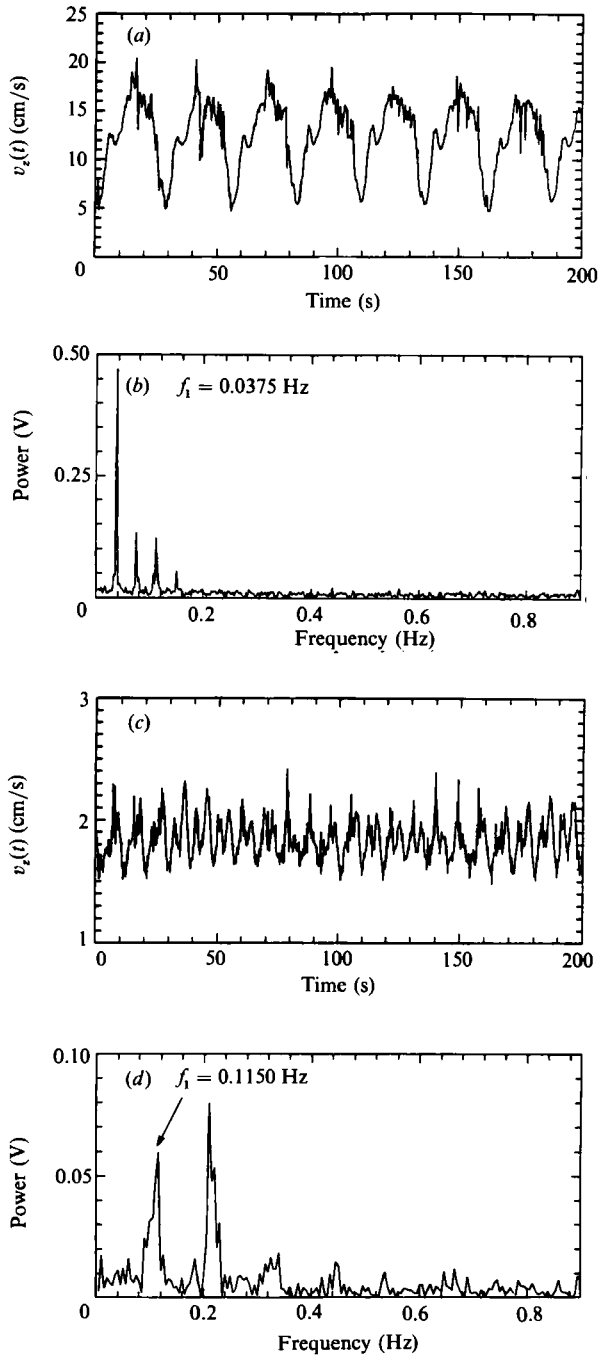

FIGURE 22. Time series and FFT spectra demonstrating different modes of oscillation for the large elastic vortex: (*a*) highly nonlinear large-amplitude oscillation in the axial velocity at $De_2 = 4.49$, $Re_2 = 0.083$ on the centreline ($\xi = 0, \zeta = -1.50$) of the 4:1 contraction; (*b*) FFT spectrum of the time series in (*a*), which gives the frequency of oscillation as $f_{\text{pulse}} = 0.0375$ Hz; (*c*) time series of the axial velocity at $De_2 = 4.33$, $Re_2 = 0.055$ on the centreline ($\xi = 0, \zeta = -1.75$) of the 5:1 contraction; (*d*) FFT spectrum of the time series in (*c*) which gives the frequency of oscillation as $f_{\text{rot}} = 0.1150$ Hz.

β	Q (cm^3/s)	$\dot{\gamma}_2$ (s^{-1})	De_2	Re_2	τ_w (kPa)	N_{1w} (kPa)	$\frac{N_{1w}}{\tau_w}$	Mode of instability
2	7.25	72.06	4.77	0.098	2.970	41.12	13.85	Pulsing
3	6.91	68.75	4.70	0.094	2.855	39.41	13.80	Pulsing
4	5.64	56.10	4.40	0.077	2.369	32.01	13.51	Pulsing
5	4.80	47.74	4.16	0.065	2.024	26.44	13.06	Rotating
6	6.19	61.57	4.53	0.084	2.596	34.65	13.35	Rotating

TABLE 3. Flow conditions at the onset of unsteady oscillations in the large upstream vortex. The oscillation mode observed in each contraction ratio is indicated in the last column. The subscript definitions are as given in table 2.

3.3.2. *Elastic vortex instability*: $2 \leqslant \beta \leqslant 6$

In addition to the local time-dependent flow dynamics observed near the lip, a separate, macroscopic flow instability is observed at high Deborah numbers. As the flow rate is increased the elastic vortex continues to grow upstream and the vortex size is found to correlate well with the downstream Deborah number, as shown in figure 2. At a Deborah number of $De_2 = 4.4$ the reattachment length in the 4:1 contraction has reached a maximum steady value of $\chi = 0.53$. Any further increase in De_2 results in the development of an unsteady vortex which remains symmetric but *pulsates* periodically in size. At $De_2 = 4.5$ the reattachment length of this vortex gradually increases with time to a value of $\chi = 0.73$ and then rapidly collapses to a much smaller, less intense vortex with $\chi = 0.48$ before increasing in size again. This periodic pulsating of the vortex is accompanied by highly nonlinear oscillations in the axial velocity, as shown in figure 22(*a*). The increasing size of the secondary recirculation in the corners of the upstream tube reduces the cross-sectional area for the primary flow through the contraction, and the axial velocity along the centreline therefore increases. When the elastic vortex stops growing in each cycle the axial velocity reaches a maximum and then decreases rapidly as the elastic vortex collapses. The FFT shown in figure 22(*b*) reveals the relatively strong contributions of the first and second harmonics to the fundamental oscillation frequency $f_{\text{pulse}} = 0.0375$ Hz. These oscillations in vortex size and axial velocity have a much lower frequency than the local dynamics observed near the lip in §3.3.1, and the period of oscillation $T_{\text{pulse}} = 1/f_{\text{pulse}}$ is much longer than the characteristic relaxation times listed in table 1 for this fluid. This instability thus does not appear to be simply connected either to the lip kinematics observed at moderate De_2 or to the specific fluid under consideration, but is a separate dynamical regime associated with the geometric size of the large upstream tube.

The dynamics of this large vortex instability is highly sensitive to the contraction ratio; the flow conditions at onset of oscillation are summarized in table 3. In the 3:1 contraction a slow pulsing in the vortex size, comparable with that described above, is observed for $De_2 \geqslant 4.3$; however, the amplitude of the oscillations is smaller and the reattachment length varies between $\chi = 0.51$–0.60. The pulsing frequency is $f_{\text{pulse}} \approx 0.055$ Hz. A similar weak pulsing instability is also observed for $\beta = 2$. In the larger contraction ratios, $\beta = 5$ and 6, a distinctly different mode of instability is observed. The large vortex becomes asymmetric with a reattachment length that varies in θ. The vortex does not pulsate and the asymmetric form of the reattachment length remains approximately constant in time; however, the vortex begins to rotate

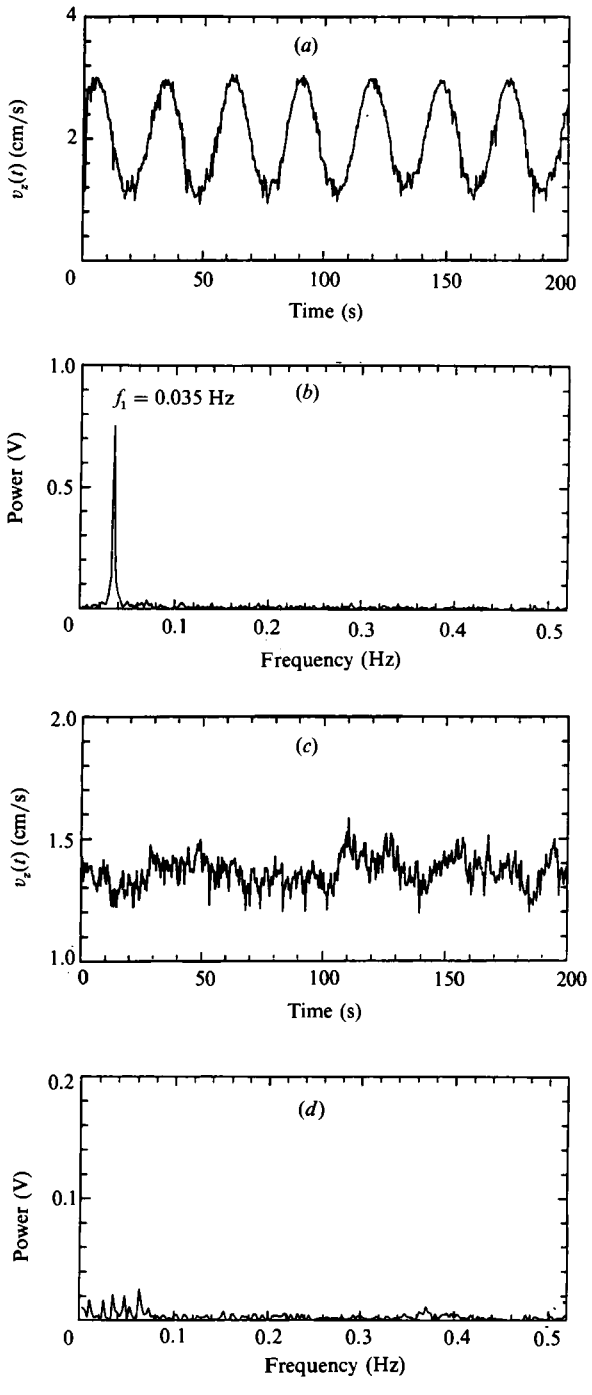

FIGURE 23. Time-dependent velocity profiles far upstream of the contraction plane: (*a*) centreline axial velocity at $\zeta = -25$ and $De_2 = 4.34$, $Re_2 = 0.076$ in the 4:1 contraction; (*b*) FFT of the time series in (*a*), which gives $f_{\text{pulse}} = 0.0350$ Hz; (*c*) the centreline axial velocity far upstream at $\zeta = -20$ and $De_2 = 4.33$, $Re_2 = 0.075$ in the 5:1 contraction; (*d*) an FFT of the data in (*c*) shows no dominant frequency of oscillation.

rapidly around the upstream tube. When a longitudinal cross-section is viewed by using the techniques described in §2.4, the two sections of the corner vortex on either side of the primary flow through the contraction alternately expand and contract in size as the position of maximum vortex size rotates around the upstream tube. This *rotating* flow regime has been clearly documented in the photographs of Nguyên & Boger (1979). Close inspection of the vortex dynamics on videotape reveals that the actual fluid particles within the vortex have no tangential velocity and that the secondary flow in the recirculating vortex remains two-dimensional. The variation in the vortex height arises from an asymmetry that develops in the streamlines of the converging primary flow and which then precesses azimuthally around the upstream tube. This azimuthal rotation results in periodic oscillations in the axial velocity along the centreline; a typical time series is shown in figure 22(*c*) for flow in a 5:1 contraction at $De_2 = 4.33$. Comparing figures 22(*a*) and 22(*c*) it is clear that the dynamics in the rotating and pulsing flow regimes are quite different with much faster oscillations observed in the 5:1 contraction. The fundamental frequency for azimuthal rotation was measured as $f_{\text{rot}} = 0.1150$ Hz by taking the lowest-frequency peak in the FFT spectrum shown in figure 22(*d*); however, the first harmonic peak ($2f_{\text{rot}}$) is of comparable intensity. The oscillation frequencies for both the pulsing and rotating flow regimes increased slowly with increasing Deborah number. With the current equipment the maximum flow rate attainable gave $De_2 \approx 4.7$ and only a few data points could be obtained in each of the time-dependent regimes. No time-dependent vortex dynamics were observed in the 8:1 contraction up to $De_2 = 4.70$; however, we believe that at higher flow rates qualitatively similar behaviour would be observed.

The oscillations in the flow associated with variations of the vortex size are not confined to the spatial region near the contraction plane, but also extend far up- and downstream. The axial velocity on the centreline at a distance $25R_2$ upstream is shown in figure 23(*a*) for $\beta = 4$. Large-amplitude fluctuations in the velocity are observed and the frequency of oscillation shown in figure 23(*b*) is the same as the pulsing frequency f_{pulse} observed near the throat of the contraction. The azimuthal rotation of the vortex that occurs for $\beta = 5$ and 6 results in less disturbance to the flow far upstream. Figure 23(*c*) shows the lower-amplitude irregular disturbances observed in the centreline velocity $20R_2$ upstream of the contraction plane for $\beta = 5$ at the same flow conditions as for figure 23(*c*). The FFT of this time series is shown in figure 23(*d*) and identifies some low-frequency components, but no clear fundamental oscillation frequency.

3.4. *The effect of lip curvature on flow dynamics*

In previous qualitative investigations of viscoelastic flow through contraction geometries the precise shape of the re-entrant corner at the contraction lip was found to have a pronounced effect on the flow characteristics. Rounding the corner resulted in a reduction in the size of the large corner vortex observed in the axisymmetric contraction flow of Boger fluids (Walters & Webster 1982) and was reported to increase the stability and reduce the size of the vortex in planar contractions (Evans & Walters 1986, 1989). A smoothly curved lip entrance was made with a fixed radius of curvature, $\mathscr{R}$, to investigate the effect of removing the sharp re-entrant corner on the local flow dynamics near the lip. The dimensionless radius of curvature of the curved lip is $\mathscr{R}/R_2 = 0.5$ and is the same as that employed by Walters & Webster. However, to prevent the introduction of asymmetry into the flow and the associated distortion of the global flow field described by Evans & Walters, the entire

(a)

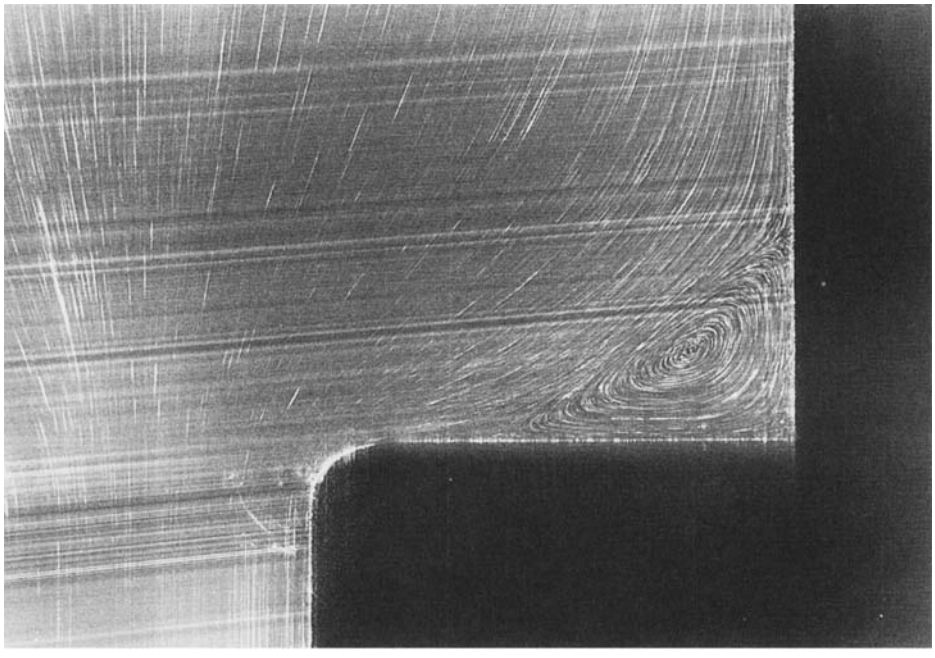

(b)

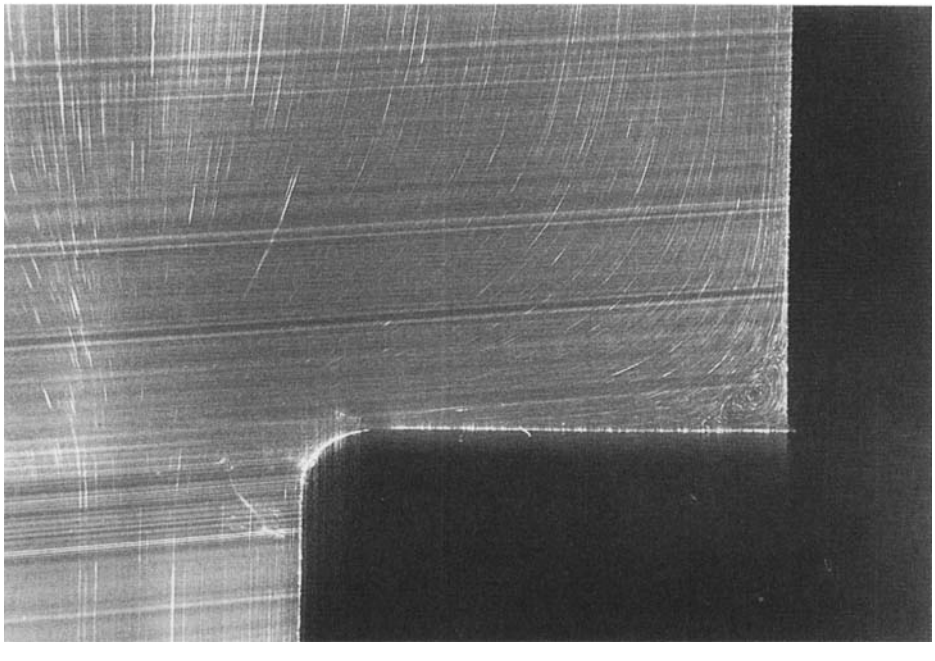

FIGURE 24(a, b). For caption see facing page.

(*c*)

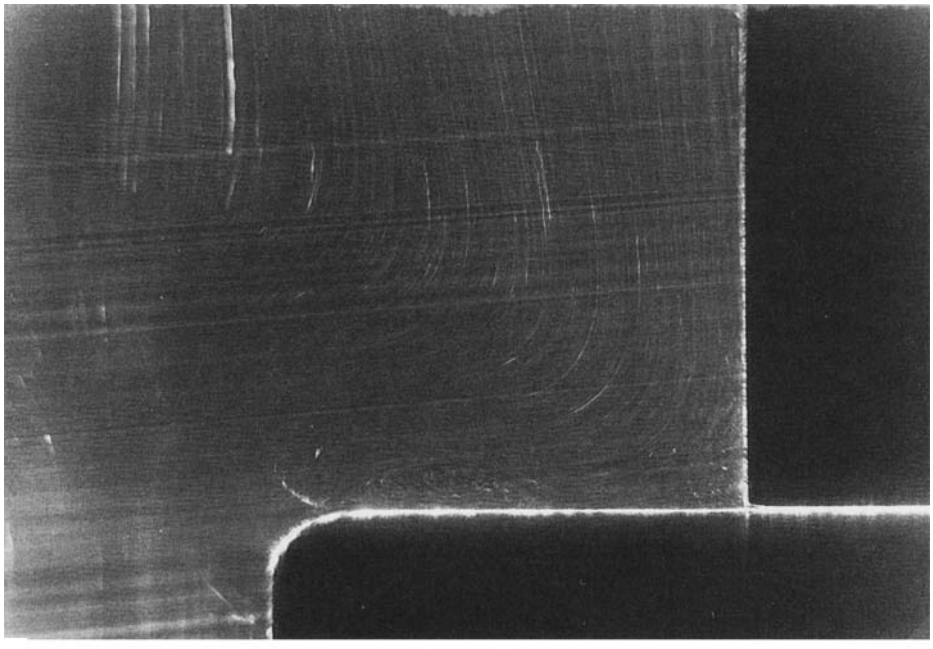

(*d*)

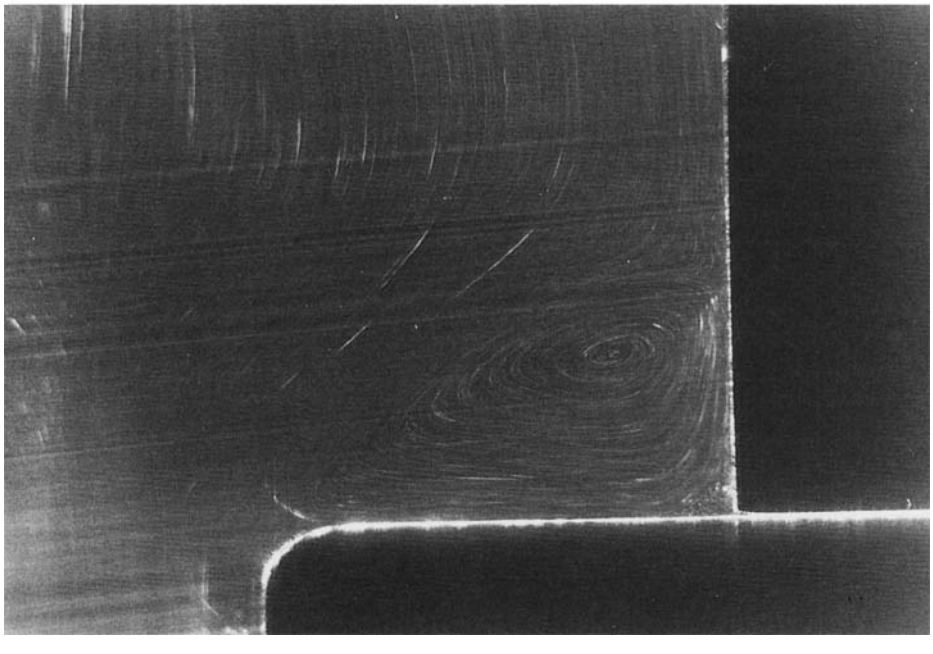

FIGURE 24. Viscoelastic flow through a 4:1 contraction with a smoothly curved entrance lip: (*a*) detailed view of the weak Moffat eddy; $De_2 = 0.56$, $Re_2 = 0.005$ (exposure time $T = 128$ s); (*b*) reduced corner vortex size; $De_2 = 3.24$, $Re_2 = 0.031$ ($T = 64$ s); (*c*) formation of a highly unsteady, time-dependent vortex near the lip entrance; $De_2 = 4.65$, $Re_2 = 0.091$ ($T = 2$ s); (*d*) elastic vortex growth regime; $De_2 = 5.32$, $Re_2 = 0.137$ ($T = 4$ s).

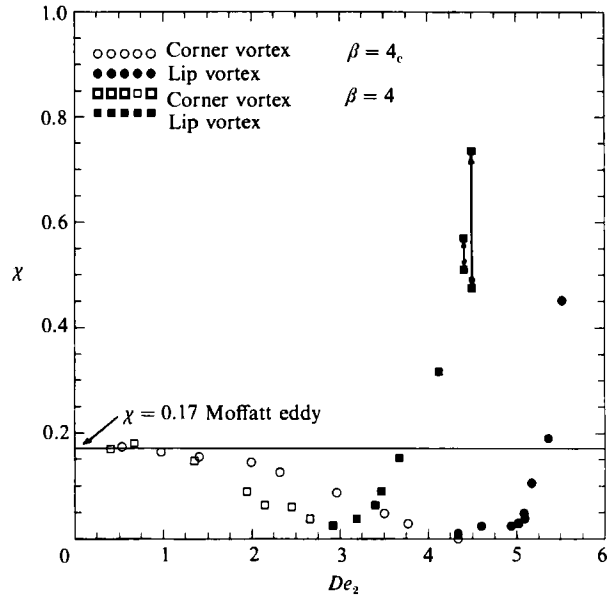

FIGURE 25. Comparison of the dimensionless vortex reattachment length (χ) for flow through a 4:1 contraction with a sharp lip ($\beta = 4$) and with a smoothly curved lip with radius of curvature $\mathscr{R} = 0.5R_2$ ($\beta = 4_c$). The hollow symbols correspond to the shrinking corner vortex, and the solid symbols represent the elastic vortex which develops near the lip edge. The arrows connecting data points at high De_2 indicate that the large vortex has become unstable and pulsates in size.

circumference of the re-entrant corner was smoothed, instead of only a 180° arc. The results presented here demonstrate that the flow transitions observed in an abrupt contraction are still present for flow through a contraction with a rounded lip, but that the critical values of Deborah number for each transition are increased because of the less severe flow conditions near the re-entrant corner of the smooth geometry.

Rounding the lip corner is found to have little effect on the flow characteristics at low De_2. A close-up of the flow patterns near the curved lip in a 4:1 contraction at $De_2 = 0.56$ is shown in figure 24(*a*). The flow converges radially towards the contraction mouth and a weak recirculating eddy, similar to that observed with the sharp lip in figure 3(*a*), is observed in the stagnant corner. The dimensionless reattachment length for the corner vortex is measured as $\chi = 0.17$. Axial and radial LDV scans are not presented here because the data superpose with the results shown in figures 5 and 6, except for the region extremely close to the smoothed corner ($-1.5 < \xi < 1.5$, $-0.3 < \zeta < 0$).

As the Deborah number is increased the consequences of smoothing the lip corner become more pronounced. The variation in vortex size (χ) with De_2 is compared in figure 25 for flow through the 4:1 contraction with a sharp lip ($\beta = 4$) and with the curved lip entrance ($\beta = 4_c$). At low Deborah numbers the reattachment length of the weak corner vortex for both lip geometries was $\chi = 0.17$. In the sharp lip geometry the corner eddy gradually decreased in size, and a separate lip vortex formed at $De_2 = 3.0$ which grew rapidly in size and engulfed the diminished corner vortex. The vortex then grew into the upstream tube and ultimately began to pulse in size at $De_2 = 4.4$ as described in §§3.1–3.3.

Similar trends were exhibited in the curved lip geometry; however, removing the lip singularity shifted the transitions to higher De_2. The corner vortex decreased in

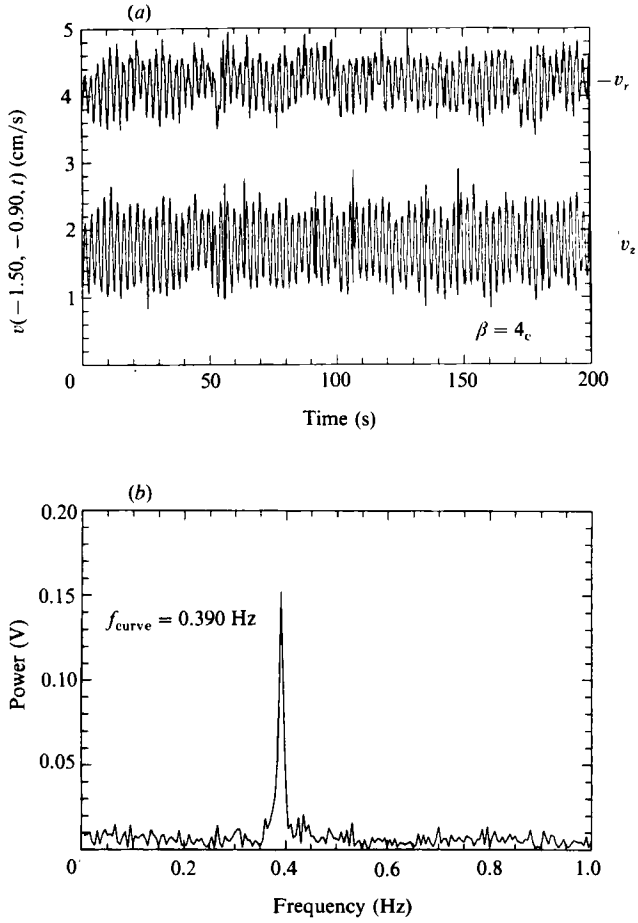

FIGURE 26. Time-dependent oscillations in the velocity near the lip of the 4:1 contraction with a curved entrance lip ($\beta = 4_c$): (*a*) the radial and axial velocity components near the lip entrance ($\xi = 1.50, \zeta = -0.90$) at $De_2 = 5.02$ and $Re_2 = 0.088$; (*b*) FFT of the axial velocity component which gives the frequency of oscillation as $f_{curve} = 0.390$ Hz.

size very gradually and had effectively disappeared by $De_2 = 4.5$ when a clearly distinct lip vortex formed. The flow field at $De_2 = 3.24$ is shown in figure 24(*b*). The weak eddy in the outer corner has greatly decreased in size, no lip vortex can be distinguished, and fluid flows smoothly around the curved lip into the downstream tube. LDV measurements also show that the flow remains steady and axisymmetric. The first flow transition observed in the curved lip geometry was the formation of a small, highly unsteady vortex near the smoothed entrance to the small tube at $De_2 = 4.50$. This time-dependent vortex expanded outwards across the base of the upstream tube and is shown in figure 24(*c*) at $De_2 = 4.65$. The lip vortex oscillated rapidly in size and was difficult to resolve with the flow visualization procedure. Figure 24(*c*) is included as the first graphic evidence of the formation of an elastic lip vortex in a contraction geometry with a smoothed lip entrance. Detailed analysis of the videotapes confirms unequivocally that this vortex originates at the lip entrance and not in the stagnant outer corners of the large tube. The oscillations in the size of the lip vortex are accompanied by rapid periodic fluctuations in the axial and

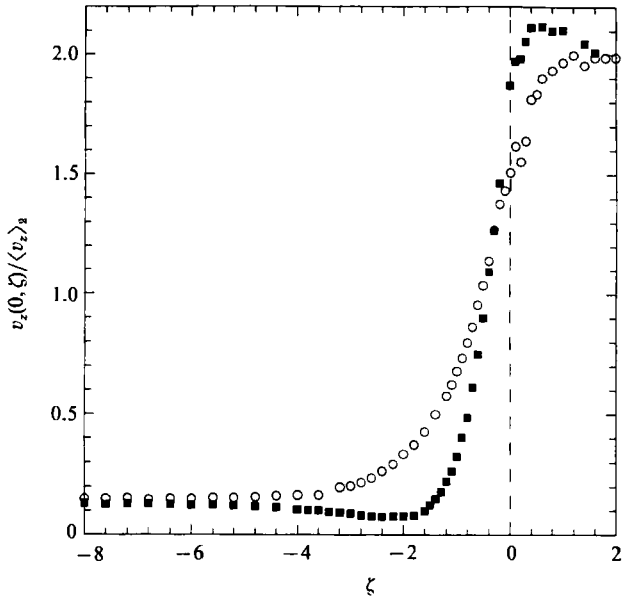

FIGURE 27. Normalized axial velocity $v_z(0,\zeta)/\langle v_z\rangle_2$ along the centreline of the 4:1 contraction with a curved entrance lip ($\beta = 4_c$): at $De_2 = 0.42$, $Re_2 = 0.004$ (○) the flow converges smoothly towards the small tube and the velocity increases monotonically; at $De_2 = 4.60$, $Re_2 = 0.08$ (■) the flow upstream of the contraction diverges from the centreline and the axial velocity shows a local minimum at $\zeta \approx -2.0$.

radial velocity components near the lip, as shown in figure 26(*a*). Both velocity components oscillate with the same frequency which was determined from the FFT data in figure 26(*b*) to be $f_{\text{curve}} = 0.390$ Hz. This frequency is much higher than the fundamental frequencies measured in any of the flows with sharp re-entrant corners.

The time-periodic lip vortex expands outwards with increasing De_2 until it reaches the upstream tube wall at $De_2 = 5.20$. At higher Deborah numbers the vortex begins to grow upstream as shown in figure 24(*d*). It is also temporally stabilized, and the flow returns to a steady two-dimensional state. At $De_2 = 5.5$ the vortex height reaches a maximum size $\chi = 0.45$ and begins to oscillate in a way similar to that described in §3.3.2. The frequency of vortex oscillation is once again found to be far more rapid ($f_c \approx 0.40$ Hz) than that observed for a sharp-lipped entrance.

At high flow rates the streamlines in the curved lip geometry were also observed to diverge outwards from the centreline, as previously described in §3.3.1 for abrupt contractions. Smoothing the re-entrant corner was found to delay this transition and, as may be seen by examining figures 24(*c*) and 24(*d*), the development of diverging flow does not occur until $De_2 \geqslant 4.5$. Sample LDV measurements of the axial velocity profile along the centreline are shown in figure 27. At low De_2 the velocity monotonically increases as the fluid approaches the contraction plane and reaches a fully developed parabolic velocity profile within one small-tube radius ($\zeta = +1$) downstream. At $De_2 = 4.60$ the data show a local velocity minimum above the contraction entrance at $\zeta \approx -2.0$ and a small velocity overshoot along the centreline just downstream of the contraction at $\zeta = +0.70$.

4. Summary and discussion

The experiments described here demonstrate a rich variety of nonlinear fluid mechanics in the contraction flow of this particular viscoelastic fluid. Flow transitions involving both steady-state, two-dimensional and time-dependent, three-dimensional motions have been documented as a function of the Deborah number of the flow and of the contraction ratio. These results are summarized on the transition diagram, figure 17, and give a rational description of the evolution of the dynamics with De_2 and β.

Any theory for describing flow transitions in the contraction geometry must produce stability curves with at least the same qualitative dependence on De and β for fluids with the same rheology. Moreover, the flow transitions for other viscoelastic fluids must be described by qualitatively similar transition curves that may be shifted by differences in the material properties of the fluid. One of the most important challenges is to understand the impact of fluid rheology on the details of the flow transitions, i.e. on the shapes and locations of the transition curves in figure 17. Both the shear and extensional characteristics of the fluid are no doubt important. The variation of $De^{(\mathrm{osc})}$, i.e. the critical Deborah number (based on the downstream flow conditions) for onset of the lip instability, with contraction ratio suggests that the upstream flow conditions also play an important role in the dynamics observed in the lip region.

The effect of shearing in the upstream tube is characterized by the wall shear rate $\dot{\gamma}_{1w} = 4\dot{\gamma}_2/\beta^3$. It is less clear which extensional parameter should be employed to characterize the behaviour observed in each contraction ratio. The LDV data presented in figures 5 and 20 show that near the contraction plane the fluid experiences approximately the same extensional strain rate $\dot{\epsilon}$ in each contraction ratio at the same value of De_2. This suggests that the total extensional strain ϵ may be a more appropriate measure for the flow as suggested by Boger (1987). The total Hencky strain experienced by fluid elements moving along the centreline is

$$\epsilon \equiv \int_0^{+\infty} \dot{\epsilon}\,\mathrm{d}t = \int_{v_z(-\infty)}^{v_z(+\infty)} \frac{\mathrm{d}v_z}{v_z} = \ln(\beta^2). \tag{6}$$

Thus the upstream shear rate and total extensional behaviour are two competing influences which vary quite differently with contraction ratio. For a given De_2, low contraction ratios will produce more highly distorted molecules in the upstream flow owing to shear, whereas higher contraction ratios will produce greater elongation of the macromolecules because of the larger Hencky strains. The differences in the flow caused by changing contraction ratio can be explained qualitatively in terms of the relative importance of shear and extensional characteristics of the fluid.

In all contraction ratios the flow structure changes from a Newtonian-like pattern as the Deborah number is increased. The shape of the weak corner eddy observed in the outer corner of the upstream tube becomes convex, the intensity of recirculation increases, and the centre of rotation shifts towards the centre of the tube as previously described by Boger (1987). In low contraction ratios ($\beta \leqslant 5$) the weak recirculation in the corner (figure 4) collapses and a time-dependent lip vortex develops that is clearly isolated from the outer tube walls. As shown in figures 3(*a*) and 24(*a*), the Moffat vortex is a weak recirculation in the outer corner of the upstream tube with a concave boundary separating it from the primary flow through the contraction. At higher De_2 this corner vortex has almost completely disappeared

and fluid streamlines near the outer walls extend down to the contraction plane, as shown in figures 3(*b*) and 24(*b*). The large elastic vortex that develops and grows upstream at higher De_2 is shown in figures 3(*b*) and 24(*c*) to originate in the immediate vicinity of the re-entrant lip corner and subsequently expands outward to the outer corner as the Deborah number is increased. This isolated lip vortex gives rise to the complex dynamics documented in §§3.2 and 3.4. At higher Deborah numbers, the significant shear rates experienced in the upstream tube for small β will lead to a shear thinning in the fluid elasticity. This shear thinning near the wall, coupled with extensional thickening along the centreline may explain why the flow upstream develops the diverging streamlines documented in figures 3(*c*) and 18. As the contraction ratio is increased the shear rate upstream rapidly decreases leading to less shear thinning and a decrease in the diverging flow. Unfortunately, to quantify these competing effects requires accurate experimental measurements of the extensional behaviour of elastic liquids and of the stress distributions throughout the contraction geometry.

In the larger contraction ratios ($\beta \geqslant 6$) the centre of rotation of the corner vortex also moves inwards as the Deborah number increases; however, the significantly lower shear rates in the upstream tube and the higher extensional strain prevent separation of the corner vortex and lip vortex. The recirculation extends across the complete contraction plane, as shown in figure 3(*d*), and the flow remains steady and two-dimensional. The presence of this recirculation coupled with the much lower shear rates in the upstream tube prevent the development of diverging streamlines, and the flow converges radially into the downstream tube at all De_2 experimentally attainable.

The differences in the dynamics of lip vortex formation between PAC/CS and PIB/PB Boger fluids reported by Boger and coworkers (Boger *et al.* 1986; Boger 1987) must arise from differences in the fluid rheology. The stability diagram for contraction flow of PAC/CS fluids may be similar to the one shown schematically in figure 17; however, the neutral stability curve for onset of the lip instability and subsequent development of an isolated time-dependent lip vortex must be shifted to the left with a minimum near $\beta = 2$. Time-dependent flows will only be observed in very small contraction ratios and for $\beta \geqslant 4$ the first flow transition will be development of a lip vortex that extends across the contraction plane and coexists with the corner vortex. Verification of such arguments requires LDV experiments in entry flows of PAC/CS fluids and reliable experimental data on the extensional properties of both fluids.

Substantial vortex growth was observed for all contraction ratios $2 \leqslant \beta \leqslant 8$. In addition, the flow visualization results have shown that in the low contraction ratios ($\beta \leqslant 5$) this large elastic vortex does not develop simply from an expansion of the weak Newtonian corner eddy that is observed at low Deborah numbers. The upstream growth of the large elastic vortex (χ) in each contraction is found to correlate well with the downstream Deborah number De_2, in agreement with the comprehensive experiments of Boger *et al.* (1986); however, this relationship does not explain the origin of the large vortices. Experiments with polymer melts (White & Kondo 1977/78; White & Baird, 1986; Piau, El Kissi & Tremblay 1988) indicate that vortex growth occurs when the fluid exhibits a large extensionally thickening elongational viscosity. This picture is consistent with the limited elongational viscosity data that is available for Boger fluids; recent experimental data for polyisobutylene-based Boger fluids suggest that the Trouton ratio varies from 100 to 1000 (Walters 1989). The nonlinear multimode constitutive equations which have

been accurately fitted to both steady and transient shear flow rheological data for the PIB/PB Boger fluid used in these experiments also predict large Trouton ratios in the range 1000–3000 (Quinzani *et al.* 1990).

The correlation of vortex growth with extensional properties, however, fails to explain the anomalous behaviour of Boger fluids in planar geometries. Experiments with polymer melts show that fluids which exhibit high extensional viscosities or unbounded stress growth give rise to substantial vortex growth in both planar, slit dies (White & Baird 1986) and in tubular, capillary dies (White & Kondo 1977/78). The picture is similar for semidilute, shear-thinning polymer solutions; the measurements of Jones *et al.* (1987) show extensional thickening in both the planar extensional viscosity $\bar{\eta}_P$ and the uniaxial extensional viscosity $\bar{\eta}_E$, while the experiments of Walters & Webster (1982) show that vortex growth also occurs in both planar and axisymmetric geometries. However, despite evidence that Boger fluids exhibit significant strain-rate thickening in both $\bar{\eta}_P$ and $\bar{\eta}_E$ (Jackson *et al.* 1984; Williams & Williams 1985), the flow visualization results of Walters and coworkers (Walters & Rawlinson 1982; Walters & Webster 1982; Binding & Walters 1988) have clearly shown that Boger fluids do *not* show any vortex growth in planar contractions. Detailed LDV and birefringence measurements for the flow of Boger fluids through planar contractions are required to explain this dichotomy. Little is known about the presence of instabilities in the planar geometry, but once again flow conditions upstream of the contraction plane must be important: for a given contraction ratio β, the upstream shear rate in a planar contraction will be higher and the Hencky strain will be lower than in the equivalent axisymmetric contraction.

At high Deborah numbers the large elastic vortex becomes unsteady and undergoes further flow transitions to macroscale time-dependent motions. By combining LDV velocity data and flow visualization we have been able to quantify two distinct modes of oscillation which are shown in figure 17. In low contraction ratios ($\beta = 2, 3, 4$) the elastic vortex remains axisymmetric but slowly pulses in vertical height with a frequency $f_{\text{pulse}} \approx 0.04$ Hz, whereas in the higher contraction ratios ($\beta = 5, 6$) a more rapid azimuthal rotation of the vortex ($f_{\text{rot}} \approx 0.10$ Hz) is observed. This azimuthal 'spiralling flow' has previously been observed in the contraction flow of shear-thinning fluids at high Reynolds number (Rama Murthy 1974; Cable & Boger 1979; Yoganathan & Yarlagadda 1984), and in the flow of a PAC/CS Boger fluid through a 7.675:1 axisymmetric contraction by Nguyên & Boger (1979). In the previous investigations little quantitative information on the vortex dynamics was presented. However, the frequency of oscillation was found to increase with flow rate and to be comparable with the values presented here. Cable & Boger (1979) reported unsteady flow of a shear-thinning polyacrylamide through a 4:1 contraction with a spiralling frequency of 0.3 Hz at a downstream wall shear rate of $\dot{\gamma}_w = 590\ \text{s}^{-1}$ which increased to 0.8 Hz at $\dot{\gamma}_w = 2500\ \text{s}^{-1}$ as the flow rate was increased.

As we have shown, these large vortex oscillations severely disturb the velocity field throughout the upstream and downstream tube and have often been compared to the instabilities encountered in the extrusion of polymer melts through a die: periodic oscillations develop in the die reservoir upstream of a contraction at stress levels in the die land of approximately 10^2 kPa and result in helical distortion of the extrudate (see for example den Otter 1970; Ballenger & White 1971; White 1973). The data in table 3 for the 4:1 contraction show that the critical Deborah number for onset of vortex oscillation is $De_2 = 4.40$ ($Re_2 = 0.077$), corresponding to a wall shear rate $\dot{\gamma}_w = 224\ \text{s}^{-1}$ and a wall shear stress of $\tau_w = 2.38$ kPa. Owing to the much lower

viscosity of polymer solutions the magnitude of the wall shear stress we observe at the onset of vortex oscillation is almost two orders of magnitude smaller than that observed in polymer melts and does not appear to be a good criterion for the development of flow instabilities. An alternative criterion that has been proposed is a critical value of the stress ratio $N_1/\tau \equiv \Psi_1 \dot{\gamma}/\eta$ evaluated at the wall shear rate in the downstream tube (Petrie & Denn 1976; Cable & Boger 1979). The stress ratio is directly proportional to our definition of the Deborah number De_2 in equation (3) and the critical value of the stress ratio at the onset of vortex oscillations is listed in table 3 for each contraction ratio. Flow transitions to a spiralling vortex regime have been observed at stress ratios of 5.3 for a monodisperse polystyrene melt (Valchopoulos & Alam 1972), between 4.5 and 5.5 for a PAC/CS Boger fluid (Nguyên & Boger 1979) and at a stress ratio of 5 for shear-thinning polyacrylamide solutions at low Reynolds number (Cable & Boger 1979). The critical stress ratios N_{1w}/τ_w given in table 3 for our PIB/PB/C14 solution are larger but of a similar magnitude to those presented in the previous investigations. In all of these studies the onset of vortex oscillations is found to occur in the 'shear-thinning' region where the stress ratio is a very weak function of shear rate. In this region, shear thinning results in a rapid decrease in the fluid elasticity (as measured by Ψ_1) and inertial effects become increasingly important.

Although we have not been able to extend our experiments beyond $De_2 \approx 6$ in any contraction geometry, it should be noted that further transitions have been reported in viscoelastic contraction flows at higher flow rates. Boger & Nguyên observed a transition at a wall shear rate $\dot{\gamma}_w$ of 300 s^{-1} from a spiralling vortex to a helical flow regime which combines elements of both of the oscillatory modes we have documented above. The large vortex becomes asymmetric, pulses vertically in height and also rotates in the azimuthal direction. Fluid particles thus follow the path of a helix into the downstream tube. At higher shear rates ($\dot{\gamma}_w = 2895$ s^{-1}) the oscillations in the upstream tube have been observed to become aperiodic for a shear-thinning polymer solution (Rama Murthy 1974). Similar large-amplitude fluctuations occur in the extrusion of polymer melts and may result in gross distortion of the extrudate or 'melt fracture'. At still higher shear rates ($\dot{\gamma}_w \approx 5000$ s^{-1}) Rama Murthy has reported a second stable regime with an extremely large steady corner vortex.

Our experiments have shown that rounding the sharp re-entrant lip corner does not prohibit the development of elastic phenomena such as a lip vortex or diverging streamlines above the contraction plane. The flow transitions are merely shifted to higher Deborah numbers. An oscillating lip vortex *is* still observed in the 4:1 contraction geometry with a smoothly curved lip, although the specific dynamic behaviour is significantly altered from that observed with the sharp lip. This suggests that the formation of an elastic lip vortex in axisymmetric contraction flows of Boger fluids reported here and by previous authors (Lawler *et al.* 1986; Boger *et al.* 1986; Boger 1987) is not directly related to the presence of a singularity in the flow, but rises from the accelerating flow near the corner. Smoothing the corner reduces the local extension rate for a given De_2 and eliminates the lip vortex, as observed by comparing figures 3(*b*) and 24(*b*). However, increasing the Deborah number in the curved lip geometry increases the extension rate and stress level near the corner and, at a sufficiently high value, a lip vortex similar to the one documented in the sharp lip geometry results. Experimentally the reduction in stresses near the lip is manifested as a lower pressure drop across the smoothed contraction entrance. Although we are not able to measure the entrance pressure drop explicitly with our apparatus, we found that for a fixed maximum pressure driving force, $\Delta P = 200$ Pa (30 p.s.i.), a higher maximum De_2 could be achieved in the curved lip geometry (see

figure 25). A further set of experiments is envisaged in which the entrance pressure drop and the critical Deborah number for formation of a time-dependent lip vortex are measured as the radius of curvature of the lip is varied.

Other modifications to the abrupt contraction geometry have been investigated in the literature, including tapering the die entrance to produce a conical converging entrance into the downstream tube. This modification to the local flow near the corner results in similar changes of the viscoelastic flow transitions to the ones we have observed by curving the lip: in polymer melts conical entrances lead to smaller amplitude oscillations of a higher frequency than those observed in a corresponding abrupt geometry (Bagley & Schreiber 1961; den Otter 1970) and in polymer solutions a lip vortex near the tapered re-entrant corner is still observed (Evans & Walters 1989). The nonlinear transitions leading to elastic vortices may be common to all viscoelastic flows with high extensional strains which result in significant elongation to the polymer chains and the development of large normal stress components in the fluid.

Our results vividly demonstrate the importance of flow near the lip of the contraction on the quantitative details of the dynamics of viscoelastic entry flows. Although a complete understanding of the relationship between these flow transitions and the details of the fluid rheology must await accurate numerical calculations, our results and the discussion of previous observations clearly show that generic flow transitions do exist in these entry flows and that the particular ordering of the transitions is a strong function of the fluid rheology.

Although numerical simulations of viscoelastic flow through abrupt contractions with a variety of differential constitutive equations have been presented, these calculations are plagued by convergence problems associated with the large velocity gradients and stresses near the re-entrant corner (see for example Mendelson *et al.* 1982; Lipscomb, Keunings & Denn 1986; Keunings 1987). Whether these difficulties are the results of computational difficulties or the inherent lack of integrability of the constitutive equations in the presence of a singularity is an unresolved problem; however, calculations with a model constructed to give an integrable singularity do converge with mesh refinement to high De (Coates *et al.* 1991). Marchal & Crochet (1987) have presented steady-state, finite-element calculations with an Oldroyd-B fluid model for flow through a 4:1 axisymmetric contraction up to a De_2 of over 50 and see the formation of a large vortex in the upstream tube at very high values of De. Unfortunately, insufficient detail is given to determine whether the vortex grew out of the Newtonian Moffat eddy or from an elastic vortex originating near the lip. This detail is important in determining the reason for the order of magnitude discrepancy in De between numerical simulations and experiments for a given vortex size (Crochet 1988).

The steady-state calculations of Coates *et al.* for the modified upper-convected Maxwell model developed by Apelian, Armstrong & Brown (1988) show the spreading of the Moffatt eddy present for the Newtonian flow and a shift in the centre of rotation towards the contraction lip as the Deborah number is increased, but do not show the formation of an independent elastic vortex near the lip. This is not surprising because the elastic lip vortex is preceded in the experiments by the transition to time-periodic flow near the lip. Calculations of time-dependent viscoelastic flows are just beginning (Northey, Armstrong & Brown 1990) and are being used to explore flow transitions in other geometries. Time-dependent, and probably three-dimensional, flow simulations will be needed to unravel computationally the details of viscoelastic contraction flows.

We are grateful to the National Science Foundation and the Office of Naval Research for their financial support of this research. We are also grateful to Lidia Quinzani for her enormous assistance in characterizing the fluid used in these experiments.

REFERENCES

APELIAN, M. R., ARMSTRONG, R. C. & BROWN, R. A. 1988 Impact of the constitutive equation and singularity on the calculation of stick-slip flow: the modified Maxwell equation (MUCM). *J. Non-Newtonian Fluid Mech.* **27**, 299–321.

BAGLEY, E. B. & SCHREIBER, H. P. 1961 Effect of die entry geometry on polymer melt fracture and extrudate distortion. *Trans. Soc. Rheol.* **5**, 341–360.

BALLENGER, T. F. & WHITE, J. L. 1971 The development of the velocity field in polymer melts in a reservoir approaching a capillary die. *J. Appl. Polymer Sci.* **15**, 1949–1962.

BERGÉ, P., POMEAU, Y. & VIDAL, C. 1986 *Order within Chaos.* John Wiley & Sons.

BINDING, D. M. & WALTERS, K. 1988 On the use of flow through a contraction in estimating the extensional viscosity of mobile polymer solutions. *J. Non-Newtonian Fluid Mech.* **30**, 233–250.

BINDING, D. M., WALTERS, K., DHEUR, J. & CROCHET, M. J. 1987 Interfacial effects in the flow of viscous and elastico-viscous liquids. *Phil. Trans. R. Soc. Lond.* A **323**, 449–469.

BINNINGTON, R. J. & BOGER, D. V. 1985 Constant viscosity elastic liquids. *J. Rheol.* **29**, 887–904.

BIRD, R. B., ARMSTRONG, R. C. & HASSAGER, O. 1987*a* *Dynamics of Polymeric Liquids*, vol. 1, 2nd edn. Wiley Interscience.

BIRD, R. B., CURTISS, C. F., ARMSTRONG, R. C. & HASSAGER, O. 1987*b* *Dynamics of Polymeric Liquids*, vol. 2, 2nd edn. Wiley Interscience.

BIRD, R. B. & DEAGUIAR, J. R. 1983 An encapsulated dumbbell model for concentrated polymer solutions and melts; I theoretical development and constitutive equation. *J. Non-Newtonian Fluid Mech.* **13**, 149–160.

BISGAARD, C. 1983 Velocity fields around spheres and bubbles investigated by laser-Doppler anemometry. *J. Non-Newtonian Fluid Mech.* **12**, 283–302.

BOGER, D. V. 1977/78 A highly elastic constant-viscosity fluid. *J. Non-Newtonian Fluid Mech.* **3**, 87–91.

BOGER, D. V. 1982 Circular entry flows of inelastic and viscoelastic fluids. In *Advances in Transport Processes*, vol. 2 (ed. A. S. Mujumdar & R. A. Mashelkar). Wiley Eastern.

BOGER, D. V. 1987 Viscoelastic flows through contractions. *Ann. Rev. Fluid Mech.* **19**, 157–182.

BOGER, D. V., HUR, D. U. & BINNINGTON, R. J. 1986 Further observations of elastic effects in tubular entry flows. *J. Non-Newtonian Fluid Mech.* **20**, 31–49.

BOGER, D. V. & NGUYÊN, H. 1978 A model viscoelastic fluid. *Polymer Engng Sci.* 18, 1037–1043.

BOGER, D. V. & RAMA MURTHY, A. V. 1972 Flow of viscoelastic fluids through an abrupt contraction. *Rheol. Acta* **11**, 61–69.

BURDETTE, S. R. 1989 Development of the velocity field in transient shear flows of viscoelastic fluids. *J. Non-Newtonian Fluid Mech.* **32**, 269–294.

CABLE, P. J. & BOGER, D. V. 1978*a* A comprehensive experimental investigation of tubular entry flow of viscoelastic fluids: part 1, vortex characteristics in stable flow. *AIChE J.* **24**, 869–879.

CABLE, P. J. & BOGER, D. V. 1978*b* A comprehensive experimental investigation of tubular entry flow of viscoelastic fluids: part 2, the velocity field in stable flow. *AIChE. J.* **24**, 882–999.

CABLE, P. J. & BOGER, D. V. 1979 A comprehensive experimental investigation of tubular entry flow of viscoelastic fluids: part 3, unstable flow. *AIChE J.* **25**, 152–159.

COATES, P. J., ARMSTRONG, R. C. & BROWN, R. A. 1991 Convergent calculations in the abrupt axisymmetric contraction using modified Maxwell models (in preparation).

CROCHET, M. J. 1988 Numerical simulation of highly viscoelastic flows. *Proc. Xth Intl Congr. on Rheology, Sydney, Australia*, vol. 1, pp. 19–24.

DEAGUIAR, J. R. 1983 An encapsulated dumbbell model for concentrated polymer solutions and melts; II. Calculation of material functions and experimental comparisons. *J. Non-Newtonian Fluid Mech.* **13**, 161–179.

EVANS, R. E. & WALTERS, K. 1986 Flow characteristics associated with abrupt changes in geometry in the case of highly elastic liquids. *J. Non-Newtonian Fluid Mech.* **20**, 11–29.

EVANS, R. E. & WALTERS, K. 1989 Further remarks on the lip-vortex mechanism of vortex enhancement in planar-contraction flow. *J. Non-Newtonian Fluid Mech.* **32**, 95–105.

FENSTERMACHER, P. R., SWINNEY, H. L. & GOLLUB, J. P. 1979 Dynamical instabilities and the transition to chaotic Taylor vortex flow. *J. Fluid Mech.* **94**, 103–128.

GIESEKUS, H. 1972 On instabilities in Poiseuille and Couette flows of viscoelastic fluids. In *Prog. Heat and Mass Transfer*, vol. 5 (ed. W. R. Schowalter, A. V. Luikov, W. J. Minkowycz & N. H. Afgan). Pergamon.

GOLLUB, J. P. & BENSON, S. V. 1980 Many routes to turbulent convection. *J. Fluid Mech.* **100**, 449–470.

HASSAGER, O. 1988 Working group on numerical techniques, fifth international workshop on numerical methods in non-Newtonian flows, Lake Arrowhead, USA. *J. Non-Newtonian Fluid Mech.* **29**, 2–5.

IOOSS, G. & JOSEPH, D. D. 1980 *Elementary Stability and Bifurcation Theory*. Springer.

JACKSON, J. P., WALTERS, K. & WILLIAMS, R. W. 1984 A rheometrical study of Boger fluids. *J. Non-Newtonian Fluid Mech.* **14**, 173–188.

JONES, D. M., WALTERS, K. & WILLIAMS, P. R. 1987 On the extensional viscosity of mobile polymer solutions. *Rheol. Acta* **26**, 20–30.

KEUNINGS, R. 1987 Simulation of viscoelastic fluid flow. In *Fundamentals of Computer Modeling for Polymer Processing* (ed. C. L. Tucker III). Carl Hanser.

KIM-E, M. E., BROWN, R. A. & ARMSTRONG, R. C. 1983 The roles of inertia and shear-thinning in flow of an inelastic liquid through an axisymmetric sudden contraction. *J. Non-Newtonian Fluid Mech.* **13**, 341–363.

LARSON, R. G., SHAQFEH, E. S. G. & MULLER, S. J. 1990 A purely elastic instability in Taylor–Couette flow. *J. Fluid Mech.* **218**, 573–600.

LAUN, H. M. & HINGMANN, R. 1990 Rheological characterization of the fluid M1 and of its components. *J. Non-Newtonian Fluid Mech.* **35**, 137–157.

LAWLER, J. V., MULLER, S. J., BROWN, R. A. & ARMSTRONG, R. C. 1986 Laser Doppler velocimetry measurements of velocity fields and transitions in viscoelastic fluids. *J. Non-Newtonian Fluid Mech.* **20**, 51–92.

LIPSCOMB, G. G., KEUNINGS, R. & DENN, M. M. 1987 Implications of boundary singularities in complex geometries. *J. Non-Newtonian Fluid Mech.* **24**, 85–96.

MACKAY, M. E. & BOGER, D. V. 1987 An explanation of the rheological properties of Boger fluids. *J. Non-Newtonian Fluid Mech.* **22**, 235–243.

MAGDA, J. J. & LARSON, R. G. 1988 A transition occurring in ideal elastic liquids during shear flow. *J. Non-Newtonian Fluid Mech.* **30**, 1–19.

MARCHAL, J. M. & CROCHET, M. J. 1987 A new mixed finite element for calculating viscoelastic flow. *J. Non-Newtonian Fluid Mech.* **26**, 77–114.

MENDELSON, M. A., YEH, P.-W., BROWN, R. A. & ARMSTRONG, R. C. 1982 Approximation error in finite element calculation of viscoelastic fluid flows. *J. Non-Newtonian Fluid Mech.* **10**, 31–54.

MOFFATT, H. K. 1964 Viscous and resistive eddies near sharp corners. *J. Fluid Mech.* **18**, 1–18.

MULLER, S. J. 1986 Experimental analysis of flow through an axisymmetric sudden contraction: Rheological characterization and LDV measurements. Ph.D thesis, Massachusetts Institute of Technology.

NGUYÊN, H. & BOGER, D. V. 1979 The kinematics and stability of die entry flows. *J. Non-Newtonian Fluid Mech.* **5**, 353–368.

NORTHEY, P. J., ARMSTRONG, R. C. & BROWN, R. A. 1990 Finite-element calculation of time-dependent two-dimensional viscoelastic flow with the EEME formulation. *J. Non-Newtonian Fluid Mech.* **36**, 109–134.

OLDROYD, J. G. 1950 On the formulation of rheological equations of state. *Proc. R. Soc. Lond.* A **200**, 523–541.

OTTER, J. L. DEN 1970 Mechanisms of melt fracture. *Plastics Polymers* **38**, 155–168.

PETRIE, C. J. S. & DENN, M. M. 1976 Instabilities in polymer processing. *AIChE J.* **22**, 209–235.

PIAU, J. M., EL KISSI, N. & TREMBLAY, B. 1988 Low Reynolds number flow visualization of linear and branched silicones upstream of orifice dies. *J. Non-Newtonian Fluid Mech.* **30**, 197–232.

PRILUTSKI, G., GUPTA, R. K., SRIDHAR, T. & RYAN, M. E. 1983 Model viscoelastic liquids. *J. Non-Newtonian Fluid Mech.* **12**, 233–241.

QUINZANI, L. M., MCKINLEY, G. H., BROWN, R. A. & ARMSTRONG, R. C. 1990 Modeling the rheology of polyisobutylene solutions. *J. Rheol.* **34**, 705–748.

RAIFORD, W. P. 1989 Laser Doppler velocimetry measurements of nonlinear viscoelastic flow transitions in the axisymmetric sudden contraction. Ph.D thesis, M.I.T.

RAIFORD, W. P., QUINZANI, L. M., COATES, P. J., ARMSTRONG, R. C. & BROWN, R. A. 1989 LDV measurements of viscoelastic flow transitions in abrupt axisymmetric contractions: interaction of inertia and elasticity. *J. Non-Newtonian Fluid Mech.* **32**, 39–68.

RAMA MURTHY, A. V. 1974 Flow instabilities in a capillary rheometer for an elastic polymer solution. *Trans. Soc. Rheol.* **18**, 431–452.

VIRIYAYUTHAKORN, M. & CASWELL, B. 1980 Finite element simulation of viscoelastic flow. *J. Non-Newtonian Fluid Mech.* **6**, 245–267.

VLACHOPOULOS, J. & ALAM, M. 1972 Critical stress and recoverable shear for polymer melt fracture. *Polymer Engng Sci.* **12**, 184.

WALTERS, K. 1989 Unpublished data on the extensional rheology of fluid M1. Presented at *6th Intl Workshop on Numerical Methods in Non-Newtonian Flows, Hindsgavl, Denmark.*

WALTERS, K. & RAWLINSON, D. M. 1982 On some contraction flows for Boger fluids. *Rheol. Acta* **21**, 547–552.

WALTERS, K. & WEBSTER, M. F. 1982 On dominating elastico-viscous response in some complex flows. *Phil. Trans. R. Soc. Lond.* A **308**, 199–218.

WHITE, J. L. 1973 Critique on flow patterns in polymer fluids at the entrance of a die and instabilities leading to extrudate distortion. *Appl. Polymer Symp.* **20**, 155–174.

WHITE, J. L. & KONDO, A. 1977/78 Flow patterns in polyethylene and polystyrene melts during extrusion through a die entry region: measurement and interpretation. *J. Non-Newtonian Fluid Mech.* **3**, 41–64.

WHITE, S. A. & BAIRD, D. G. 1986 The importance of extensional flow properties on planar entry flow patterns of polymer melts. *J. Non-Newtonian Fluid Mech.* **20**, 93–101.

WHITE, S. A., GOTSIS, A. D. & BAIRD, D. G. 1987 Review of the entry flow problem: experimental and numerical. *J. Non-Newtonian Fluid Mech.* **24**, 121–160.

WILLIAMS, P. R. & WILLIAMS, R. W. 1985 On the planar extensional viscosity of mobile liquids. *J. Non-Newtonian Fluid Mech.* **19**, 53–80.

WUNDERLICH, A. M., BRUNN, P. O. & DURST, F. 1988 Flow of dilute polyacrylamide solutions through a sudden planar contraction. *J. Non-Newtonian Fluid Mech.* **28**, 267–285.

YOGANATHAN, A. P. & YARLAGADDA, A. P. 1984 Velocity fields of viscoelastic fluids in sudden tubular contractions. *Proc. IX Intl Congress on Rheology, Acapulco, Mexico, Advances in Rheology*, vol. 2 (ed. B. Mena, A. García-Rejón & C. Rangel-Nafaile), pp. 135–142.